# Monolayer Doping of Silicon through Grafting a Tailored Molecular Phosphorus Precursor onto Oxide-Passivated Silicon Surfaces

*Thibault Alphazan,[†‡§] Laurent Mathey,[†‡§] Martin Schwarzwälder,[∥] Tsung-Han Lin,[∥] Aaron J. Rossini,[⊥] Raphaël Wischert,[∥] Virginie Enyedi,[†‡] Hervé Fontaine,[†‡] Marc Veillerot,[†‡] Anne Lesage,[⊤] Lyndon Emsley,[⊥] Laurent Veyre,[§] François Martin,[†‡] Chloé Thieuleux,[§]* and Christophe Copéret[∥]**

[†] Univ. Grenoble Alpes, F-38000 Grenoble, France.

[‡] CEA, LETI, MINATEC Campus, F-38054 Grenoble, France.

[§] C2P2, CPE Lyon, 43 Bd du 11 Nov. 1918, 69616 Villeurbanne cedex France

[∥] ETH Zürich, Department of Chemistry and Applied Biosciences, Vladimir Prelog Weg. 1-5, CH-8093 Zürich, Switzerland

[⊥] Institut des Sciences et Ingénierie Chimiques, Ecole Polytechnique Fédérale de Lausanne (EPFL), CH-1015 Lausanne, Switzerland

[T] Centre de RMN à Très Hauts Champs, Institut de Sciences Analytiques (CNRS/ENS Lyon/UCB Lyon

**ABSTRACT.** Monolayer doping (MLD) of silicon substrates at the nanoscale is a powerful method to provide controlled doses of dopants and defect-free materials. However, this approach requires the deposition of a thick $SiO_2$ cap layer to limit dopant evaporation during annealing. Here, we describe the controlled surface doping of thin oxide-passivated silicon wafers through a two-step process involving the grafting of a molecular phosphorus precursor containing a polyhedral oligomeric silsesquioxane (POSS) scaffold with silica-like architecture, and thermal annealing. We show that the POSS scaffold favors the controlled formation of dopant-containing surface species with up to ~$8 \times 10^{13}$ P atoms $cm^{-2}$, and efficiently avoids phosphorus evaporation during annealing for temperatures up to 800 °C. Silicon doping is demonstrated, in particular, by grafting the POSS phosphorus triester on $SiO_2$/Si wafers with optimized surface preparation (thin $SiO_2$ layer of 0.7 nm) and annealing temperature (1000 °C), which provides phosphorus doses of ~$7 \times 10^{12}$ P atoms $cm^{-2}$ in the silicon substrates together with a decrease of their sheet resistance. A detailed study of the surface chemistry on $SiO_2$ nanoparticles used as a high surface area model yields the grafting mechanism and the structure of the surface species. We show that the POSS scaffold is conserved upon grafting, that its size controls the final P-surface density and that it behaves as a self-protecting ligand against phosphorus volatilization during the annealing step. We thus demonstrate that the use of tailored-made dopant precursors with self-capping properties is a promising approach to tune medium to low doping doses in technologically relevant semiconductors.

## INTRODUCTION

The electrical activation of semiconductors is achieved by the incorporation of impurities (dopants) into their crystal structures. The role of dopants in advanced semiconductor devices is therefore a major field of study[1–3] whether it applies to microelectronics,[4,5] photovoltaics,[6] semiconductor lasers,[7] nanowires and sensors.[8,9] Improving the incorporation of dopants, for ultra-shallow to medium doping ranges, represents a significant challenge nowadays, in particular with the advances in materials, processing, and architectural design of nano-sized devices.[10] Amongst several methods such as ion implantation,[11] spin-on doping[12] or single-atom doping,[13] the monolayer doping (MLD) technique is very attractive and has yielded promising results.[14–18] This methodology is based on the deposition of dopants using molecular precursors on H-terminated (silicon) surfaces to form (mono)layers of surface species. The functionalization of technologically relevant surfaces like silicon, germanium and others has been widely studied,[19–21] offering versatile properties to resulting materials[22–24] and allowing for a better understanding of grafting or doping mechanisms.[25–27] However, while MLD allows for conformal coatings and a fine tuning of the organic film properties, a main road-block to its development for electronic materials is the necessity of depositing of a thick $SiO_2$ ad-layer cap on the molecular layer, to ensure dopant diffusion into the substrate (up to solid solubility) rather than its volatilization upon annealing. To circumvent this capping issue, the monolayer contact doping (MLCD) concept was recently proposed[28,29] and had shown encouraging results in the formation of (ultra)shallow junctions. Nevertheless, this *ex-situ* technique requires one donor and one acceptor substrate and is therefore less straightforward than MLD, which requires only one substrate. On oxide surfaces, the preparation of well-defined species with a controlled density of site has been extensively studied in other fields like catalysis[30–33] and functional materials,[34–37] but this concept has only been rarely applied to microelectronics.[36,38–42] In particular, it has been shown that the structure of the molecular precursors, that is the chosen

scaffold bound to the dopant, allows tuning of their surface density. In combination with the self-capping properties of these precursors, this approach has recently opened new avenues to limit dopant evaporation upon annealing and generate *p-n* junctions.[39] However, more robust scaffolds are needed to favor the diffusion of phosphorus or heavier *n*-dopants (such as antimony) into semiconductors, rather than their volatilization.

In this work, we describe the *n*-doping of silicon by a two-step process involving i) controlled grafting of a tailored-made molecular precursor onto the $SiO_2$ layer present at the surface of silicon wafers without the need of HF treatment, and ii) the rapid annealing of the materials, without using an additional thick silica-cap layer. The advantage of the chosen molecular phosphorus precursor, *i.e.* the hepta-isobutyl-polyhedral oligomeric silsesquioxane triester of phosphorus (**POSS-P**),[43] stems from the large and robust silica-like architecture of the silicon-containing ligand.[44] In particular, **POSS-P** allowed both the tuning of the dopant surface concentration by steric constraints and the protection of the phosphorus atoms up to 1000°C, avoiding dramatic volatilization. The latter property arises from the silica-like capping cage of the precursor, which generates a $SiO_2$ nano-layer upon oxidative thermal treatment. Infrared (IR) and $^{31}P$ dynamic nuclear polarization surface-enhanced NMR spectroscopy (DNP-SENS),[45–47] were combined with DFT calculations to characterize the structure of surface species using silica nanoparticles (NPs) as models for the surface chemistry of $SiO_2$/Si wafers. This study provided a detailed molecular understanding of the phosphorus doping steps, *i.e.* the role of the POSS scaffold. Optimizing the phosphorus incorporation into silicon was also demonstrated through controlling critical parameters such as the $SiO_2$ thickness and the annealing temperature, and yielded electrically active materials.

## EXPERIMENTAL SECTION

All experiments, otherwise stated, were carried out under dry and oxygen-free Ar atmosphere using either standard Schlenk or glovebox techniques for organic synthesis. For preparation and treatments of surface species, reactions were carried out using high vacuum lines ($10^{-5}$ mbar), unless specified. Further details are available in the Supporting Information.

**Dehydroxylation of $SiO_2$/Si wafers at 500 °C.** Wafers were cut into 20 cm² (2.5×8 cm²) pieces, calcined for 5 h under air at 500 °C (6 °C.min$^{-1}$), partially dehydroxylated at 500 °C under high vacuum ($10^{-5}$ mbar) for 12 h and stored in the glovebox.

**Thermal treatment of $SiO_2$/Si wafers at 140 °C.** Wafers pieces (20 cm²) loaded into a reactor which was immediately evacuated, were heated at 140 °C (6 °C.min$^{-1}$) under high vacuum ($10^{-5}$ mbar) for 17 h and then stored in the glovebox.

**Grafting of POSS-P on wafers.** After solubilizing **POSS-P** in toluene or pentane (~45 mL), the solution was contacted with the wafer pieces and left to react for 2 hours. After removing the solution, the wafers pieces were washed 3 times with toluene or pentane (~5 mL each time) before drying *in vacuo*.

**Ellipsometric measurements.** Ellipsometric data were acquired using a phase modulated ellipsometer (UVISEL from Horiba) at 70° incidence angle. Because of the unknown optical properties of the films and their nanometer thickness, data were modeled using a single layer model consisting of $SiO_2$ on silicon substrate with tabulated optical constants.

**RTP (spike) annealing of wafers.** Wafers were placed on a 20 cm diameter Si holder in the furnace, where the atmosphere was evacuated to work under a low $N_2$ pressure (200 sccm). Infrared lamps were used to warm up the furnace until the temperature remained stable at 300 °C. Then, the chamber was heated up to 985 °C (10 °C.s$^{-1}$) for 4 s, before reaching 1000 °C for 1 s. The furnace was then cooled down to room temperature.

**ICP-MS measurement of the silica thin layer covering wafers.** The vapor phase decomposition (VPD) method, as described in the literature, was used in order to measure the phosphorus content of the silica layer.[48–50] The condensation and trace metals present on the etched wafer were collected by a 0.1 mL drop of a solution of $HNO_3$ 50%. The droplet was then dropped into a small Teflon vial and the volume was adjusted to 1 mL. The resulting solution was further analyzed by inductively coupled plasma mass spectrometry (ICP-MS).

**Time of flight SIMS measurement.** SIMS analyses were performed with an impact energy ($Cs^+$ beam) of 250 eV for phosphorus depth profiling. The concentration of phosphorus was determined from RSFactors relative to the $^{30}Si$ signal established from a reference sample analyzed in the same conditions. Wafer pieces freshly cleaned with HF were cut into 1×1 cm² samples and stored in the glovebox before analysis.

**Sheet resistance measurements.** Sheet resistance was measured using a four-point probe setup (Resmap, CDE). All samples were treated by dipping into 10% HF solution for 3 min, rinsing with deionized water and drying before measurement.

## RESULTS AND DISCUSSION

### Grafting of molecular phosphorus precursors onto $SiO_2$ NPs and $SiO_2$/Si wafers

The molecular phosphorus precursor (**POSS-P**), prepared according to a literature procedure,[43] was first grafted onto silica particles (Ø ≈ 20 nm, 197 $m^2 g^{-1}$), partially dehydroxylated at 500 °C, which have an OH density of *ca*. 2.0 OH $nm^{-2}$ (*i.e* 200 × $10^{12}$ OH $cm^{-2}$).[51] The resulting solid – **POSS-P/$SiO_{2-(500)}$** – contains 0.47 wt % of phosphorus, which corresponds to 0.46 P atoms $nm^{-2}$ (or 46 × $10^{12}$ P atoms $cm^{-2}$) and the consumption of only *ca*. 23% of the surface anchoring groups (≡SiOH). Considering that the maximal density of P atoms (ideal monolayer) should be close to this of Si atoms in silica (10 Si atoms $nm^{-2}$), the large projected surface area (footprint) of **POSS-P** (~1.5 $nm^2$, *i.e*. ~ 0.7 P atoms $nm^{-2}$) ensures a

surface density far below a monolayer. The absence of recovery of **POSS-P** upon thorough washings with a coordinating solvent like THF indicates that the molecular precursor is bound to the silica surface and not only physisorbed. The partial consumption of surface OH upon grafting of P-species is confirmed by IR (Figure 1A), as evidenced by the presence of remaining isolated (3746 $cm^{-1}$) and perturbed (H-bonded, 3703 $cm^{-1}$) surface silanols, likely interacting with the adsorbed POSS cage associated with the appearance of ν(C-H) vibration bands from the isobutyl chains. The two bands appearing at 2450 and 2425 $cm^{-1}$ ($\Delta\nu \sim 25$ $cm^{-1}$) are assigned to ν(P-H) bands[52] of $P^{V}$(=O)H species in slightly different environments (Figure S2 and Table S3). This attribution is confirmed by the appearance of the corresponding red-shifted bands at 1786 and 1760 $cm^{-1}$ (ν(P-D)) upon grafting POSS-P on deuterated silica (≡SiOD). **POSS-P** thus grafts onto the silica surface *via* an Arbuzov-type rearrangement, generating surface species with a $P^{V}$(=O)(H) group as shown in Scheme 1.[53] In addition, the presence of a broad band centered at about 3300 $cm^{-1}$ shows that the grafted P-species interacts *via* hydrogen-bonding with remaining ≡SiOH groups. We then investigated their structure by solid-state NMR spectroscopy. However, the relatively low density of P atoms combined with the large chemical shift anisotropy (CSA) of P-species made the acquisition of high quality spectra by conventional magic angle spinning (MAS) NMR difficult; we thus used DNP-SENS[45–47] to improve signal/noise ratios. DNP enhanced $^{31}$P solid-state NMR spectroscopy was performed on **POSS/SiO$_{2-(700)}$** (Figure 1B) to identify the different surface P-species. The DNP-SENS $^{31}$P cross-polarization (CP) MAS spectrum shows one major P species at about -16 ppm and a minor species at about -3 ppm. The major species is attributed to a $P^{V}$(=O)(H) center[54] still anchored to two siloxy groups of the POSS cage, which was opened upon grafting onto surface ≡SiOH groups. The minor species shows similar spectroscopic signatures, pointing to a structure in a slightly different environment, probably arising from H-bonding to remaining silanols (Scheme

1 and Figure S2). The large signal enhancement resulting from the use of DNP-SENS allows measurement of the CSA parameters by fitting the sideband manifolds of NMR spectra extracted from two-dimensional magic angle turning experiments (MAT, Figure S4): the major species at *ca*. -16 ppm is found to have a span (Ω) of 185 ppm and an asymmetry parameter (κ) of 0.5, while the minor species at *ca*. -3 ppm is associated with Ω = 156 ppm and κ = 0.27. DFT calculations on molecular analogues (see Supporting Information) show that the presence of adjacent silanols interacting with the P(=O)H unit leads to a downfield shift of *ca*. 12 to 18 ppm and a reduction of the span, in agreement with experiment, thus confirming our previous assignments. This interpretation is also consistent with the presence of two P-H vibration bands in the IR spectrum and the calculated frequency shift resulting from the interaction of an ≡SiOH with P(=O)H (Table S3). Moreover, the $^{29}$Si CP-MAS NMR (Figure S5) spectrum reveals the presence of $T_3$-like Si atoms of the POSS cage (–66 ppm) and of Q-type Si atoms of the silica support (around –100 ppm). The absence of $T_2$-type $Si_{POSS}$-OH at –57 ppm confirms that the structure of the POSS scaffold was preserved upon grafting. Finally, the DNP enhanced 2D $^{29}$Si-$^{31}$P correlation spectrum shows a single correlation between the T-type silicons and phosphorus (Figure S6), consistent with the proposed structure of Scheme 1. Similar results are obtained when grafting **POSS-P** on silica particles partially dehydroxylated at 700, 500 and 140 °C (see Supporting Information), thus confirming that the phosphorus density is governed by the steric hindrance of surface P-species. For comparison, grafting diethyl-benzyl phosphonate (DEBP, projected area ~2.6-fold lower) or p-tosylate tributyl-ethylphosphonium (TBEP, projected area ~1.6-fold lower) under similar conditions ($SiO_{2-(700)}$ NPs) allows reaching significantly higher P–contents of ~ 1.0 and ~ 0.6 P atoms nm$^{-2}$, respectively. The dopant dose on the surface can thus be finely tuned by adjusting the size of the P-precursor, as an alternative to mixed monolayer doping.[55]

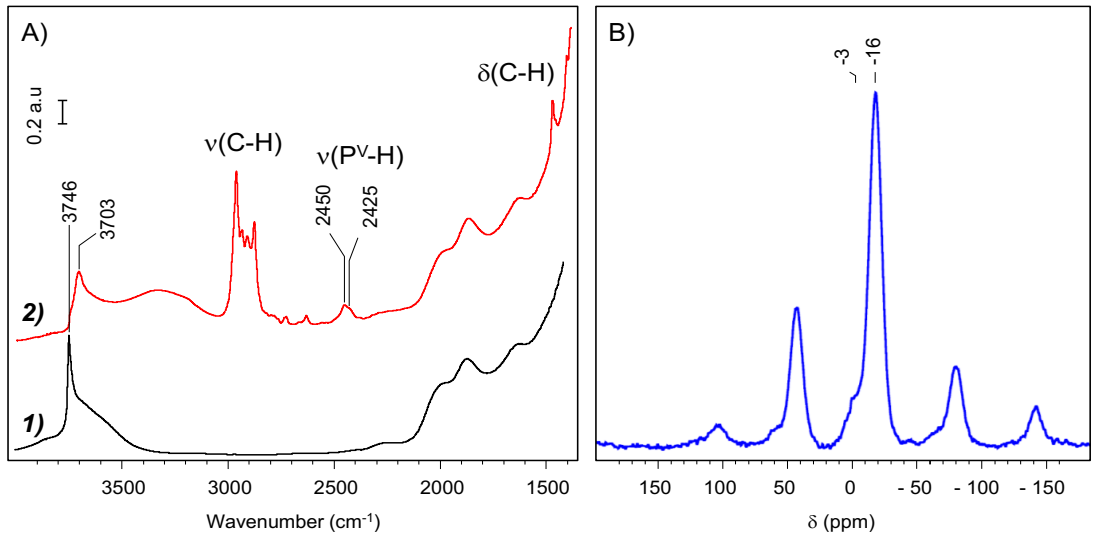


**Figure 1**: (A) IR spectra of $SiO_{2-(500)}$ NPs (1) and $SiO_{2-(500)}$-supported POSS-P (2). (B) DNP-SENS $^{31}P$ CP-MAS NMR spectrum of $SiO_{2-(700)}$-supported POSS-P.

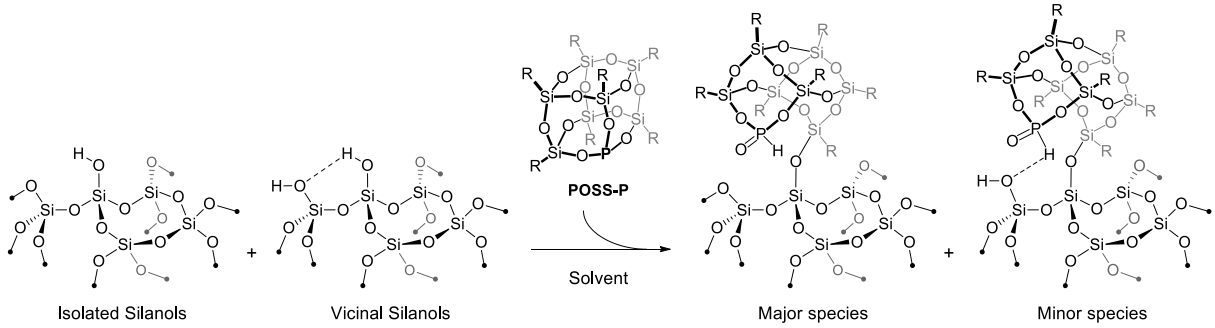


**Scheme 1**: Proposed structure of surface species formed by grafting POSS-P onto silica partially dehydroxylated at 500 °C. R stands for isobutyl chains.

We then transferred this methodology to silicon wafers covered with a thin oxide layer (0.7 to 1.5 nm). Following thermal treatment similar to that used for $SiO_2$ NPs, *p*-type low-doped Si wafers were contacted with a 80 $\mu$M solution of **POSS-P** in pentane or toluene, and thoroughly rinsed to yield **POSS-P/Wafer**. The phosphorus content of the oxide layer of each wafer was quantified by VPD, followed by ICP-MS. Values of $42.8 \pm 8.8 \times 10^{12}$ and $85.0 \pm 14.0 \times 10^{12}$ P atoms $cm^{-2}$ (*i.e* between 0.4 and 0.8 P atoms $nm^{-2}$) were measured for wafers treated at 140 and 500 °C, respectively. Characterizing the chemisorbed POSS-P onto the thin oxide layer (P-O(Si) and P=O features) by simple transmission IR analyses[26,27,56] was however not possible in

our case, due to the very low amount of P species on the surface (submonolayer of *ca*. 0.6 P $nm^{-2}$ < 10 P atoms $nm^{-2}$ for a monolayer). Complementary ellipsometry measurements and X-ray photoelectron spectroscopy (XPS) analysis (Figure S1-1 and S1-2) confirmed the presence on the passivated semiconductor surface of phosphorus surface species whose structures were unraveled with the use of silica NPs models (*vide supra*).

**Stability of surface species upon inert or oxidative thermal treatment**

Here, prior to using these surface species as dopant through thermal annealing, we first investigated their stability using the silica nanoparticle model, in order to evaluate i) the protective properties of the POSS scaffold (self-capping), and ii) the possibility to embed P atoms into an *in-situ* generated nano-$SiO_2$. Inert and oxidative thermal treatments of $SiO_2$ NP-supported materials were thus studied by *in-situ* IR coupled with GC/MS (Figure S7), IR (Figure 2) and NMR (Figure S5 and Figure S8). After heating **POSS-P/SiO$_{2\text{-}(500)}$** under argon (500 °C, 2 h), 100% of its initial phosphorous content is recovered. The slight carbon loss (~5%) that is quantified is consistent with the small decrease of ν(C-H) bands observed by *in-situ* IR. Detecting $C_3$ and $C_4$ alkenes from ~400 °C corroborates the appearance of a ν(Si-H) band from 500 °C, which thus illustrates the partial decomposition of the POSS isobutyl chains. Vibration modes assigned to P-H bonds at 2425 and 2450 $cm^{-1}$ start to change from ~150 °C, and are then shifted to 2460 $cm^{-1}$ after thermal treatment (Figure 2-1 and Figure S7-1), indicating a change of environment around the phosphorus atoms. Interestingly, direct excitation $^{31}$P MAS NMR (Figure S8) analysis reveals the presence of a new P-species (108 ppm), assigned to P atoms inserted in the silica support framework.[51] Another species (-19 ppm), which still contains the POSS scaffold and the $P^V$(=O)H group (*vide supra*), probably exhibits a structure similar to the starting surface P-species: these results underline the self-capping potential of **POSS-P**, provided by the robustness of the POSS scaffold under inert atmosphere. Besides, oxidizing **POSS-P/SiO$_{2\text{-}(500)}$** under dry air (500 °C, 2 h) yields a solid retaining phosphorus (~100%), while removing most of the carbon (>97%). Major decomposition products were propene, acetone,

and various $C_1$ to $C_4$ oxygenated alkanes/alkenes, detected from ~230 °C. From this temperature, the bands assigned to C-H bonds significantly decrease until 500 °C (Figure S7-2), which thus confirms the almost complete disappearance of the isobutyl chains of the POSS cage, consistent with carbon analyses. Vibration modes assigned to P-H bonds starts to change from ~150 °C: the two bands at 2425 and 2450 $cm^{-1}$ decrease and then totally disappear at 500 °C, which shows that surface species do not contain P-H bonds anymore. Observing a band at ~3671 $cm^{-1}$ (Figure 2-2), tentatively attributed to a PO-H vibration, is consistent with phosphorus oxidation. IR, and solid-state NMR analyses (Figure S8), support the formation of $(\equiv Si\text{-}O)_2P(=O)OH$ species among less defined $PO_x$ ones, embedded into the silica layer generated by the oxidation of the POSS scaffold.[58] In sharp contrast, a similar oxidative thermal treatment of the phosphonate (**DEBP**) or the phosphonium salt (**TBEP**) grafted on $SiO_2$ NPs leads to phosphorus losses of 86% and 62% of the starting amount, respectively: the **POSS-P** molecule thus provides enhanced protection for dopant atoms (self-capping). Note that transferring this oxidation step to **POSS-P/wafer** led to phosphorous loss of ~20%. While not fully ascertained, this result observed on wafer, but not on NPs, could originate from the different morphology of samples, in particular the low surface area associated with lower adsorption properties and/or the types of $SiO_2$.

Overall, the high stability of surface species generated by POSS-P, by comparison with the low stability of phosphonates (**DEBP**) or phosphonium salts (**TBEP**), illustrates the self-capping properties provided by the POSS scaffold, thus making POSS-P a promising dopant precursor for subsequent wafer annealing.

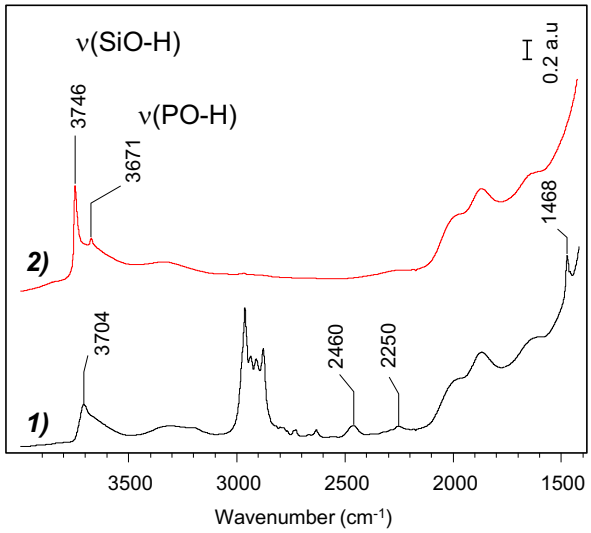


**Figure 2**: IR spectra of POSS-P/$SiO_{2-(500)}$ decomposed under argon (1) or dry air (2). Conditions: 500 °C, 2 h, 50 mL/min.

**High temperature annealing of POSS-P on thin silica covered wafers.**

We investigated the influence of the temperature on P diffusion in rapid thermal processing (RTP) of $SiO_2$/Si wafers oxidized at 500 °C for 2 h in dry air, prior to annealing. The results shown in Table 1 reveal that ~90% of the phosphorus atoms previously embedded into the nano-$SiO_2$ layer (30.7 × $10^{12}$ P atoms $cm^{-2}$) remain on the surface after RTP at 800 °C (spike 1 s). Taking the low phosphorus amount that has crossed the $SiO_2$/Si interface (2.0 × $10^{12}$ P atoms $cm^{-2}$, *i.e.* 6%) into account, ~96% of the initially grafted phosphorus dose is kept in the sample. This result obtained on $SiO_2$/Si substrates is very encouraging as the low dopant dose found in Si at 800 °C is close to literature data (5.5 × $10^{12}$ P atoms $cm^{-2}$) obtained at higher temperature (900 °C) on H-terminated silicon, using a 50 nm thick $SiO_2$ cap layer.[17] Here, P atoms, although not directly anchored to the silicon surface, obviously benefit from the protection provided by the thin layer of $SiO_2$ (~100 times thinner than previously reported).[17] Upon increasing the RTP temperature to 1000 °C the total phosphorus content (in $SiO_2$ and Si) is reduced to ~32% and a 3-fold increase in silicon doping is measured, compared to that obtained after the 800 °C

annealing step ($6.1 \times 10^{12}$ P atoms $cm^{-2}$). Hence, diffusion of a significant amount of phosphorus through the interfacial oxide competes with its evaporation through the nano-$SiO_2$ cap (<1 nm) at 1000 °C (Figure 3A). The use of phosphorus precursors with Si-containing scaffolds such as POSS is therefore a potential solution for MLD of semiconductors requiring annealing temperature below ~800 °C.

We then studied the influence of the oxide layer's thickness on the balance between evaporation and diffusion (doping). POSS-P was grafted on wafers with a silica thickness of about 0.7 nm, 0.9 nm (chemically grown oxides) and 1.5 nm (native oxide), and annealed without oxidative pre-treatment to avoid possible $SiO_2$ underlayer densification. SIMS analyses (Figure 3B and Table 1) show that 16% of the initial P content ($7.0 \times 10^{12}$ P atoms $cm^{-2}$) diffuses into Si through 0.7 nm of silica, while only 8% and less than 2% diffuse through the 0.9 nm and 1.5 nm thick silica layers, respectively. Roughly, a total amount of $10 \times 10^{12}$ P atoms $cm^{-2}$ of phosphorus stays dispersed in $SiO_2$ and Si except on the thicker oxide, probably originating from the lower transitory diffusion of phosphorus in denser oxides, which results in phosphorus being more available for evaporation. Grafting optimized self-protected dopant precursors such as POSS-P on silicon supported thin (≤ 0.7 nm) and low density chemically grown oxides thus provides an alternative solution to conventional MLD of deglazed silicon using less sophisticated molecules.

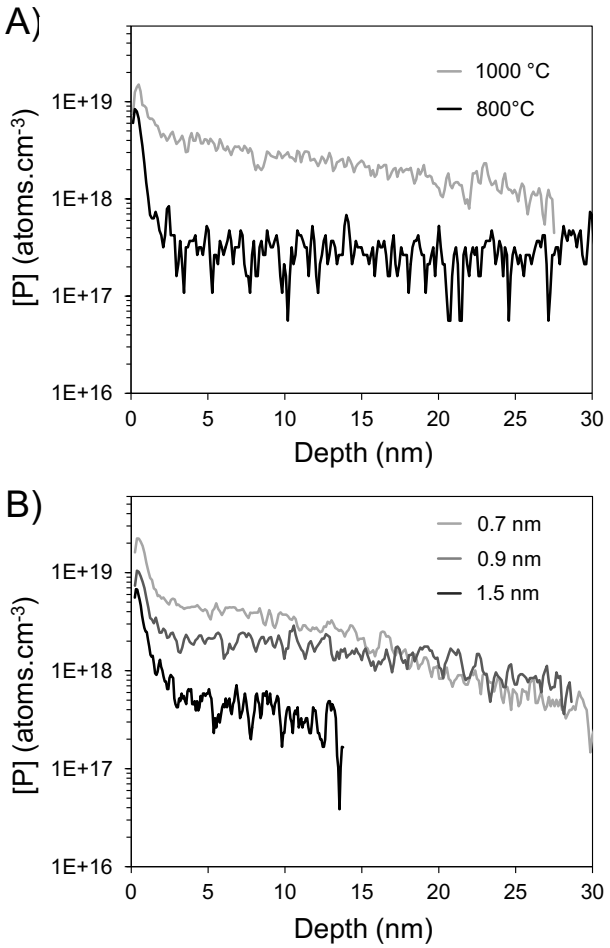


**Figure 3**: SIMS depth profiles of phosphorus dopant atoms in silicon wafers with a ~0.7 nm layer of $SiO_2$ and annealed at 800 or 1000 °C (1 s) after oxidative pre-treatment (A), and wafers with a 0.7 nm, 0.9 nm and 1.5 nm layer of $SiO_2$, annealed at 1000 °C (1 s) without oxidative pre-treatment (B).

**Table 1**: Phosphorus content of the silica layer (VPD-ICP-MS) and the silicon matrix (SIMS) of POSS-P grafted or oxidized (500 °C, 2 h, dry air) wafers, as a function of RTP conditions and $SiO_2$ thickness.

| Sample | RTP (°C) | P content ($\times 10^{12}$ P.cm$^{-2}$) In $SiO_2$[c)] | in Si[d)] | % P recovered in Si | Overall recovery (%) |
|---|---|---|---|---|---|
| Grafted + calcined[a)] | - | 34.3 | - | - | 100 |
| 0.7 nm $SiO_2$ | 1000 | 4.9 | 6.1 | 18 | 32 |
| 0.7 nm $SiO_2$ | 800 | 30.7 | 2.0 | 6 | 95 |
| Grafted[b)] | - | 42.8 | - | - | 100 |
| 0.7 nm $SiO_2$ | 1000 | 2.2 | 7.0 | 16 | 21 |
| 0.9 nm $SiO_2$ | 1000 | 8.5 | 3.6 | 8 | 28 |
| 1.5 nm $SiO_2$ | 1000 | 4.6 | < 1.0 | 2 | 13 |

a) "Calcined" stands for "oxidized" (dry air) at 500°C for 2 h

b) Average value of P content found on wafers (VPD-ICP-MS) with 0.7, 0.9 and 1.5 nm thick $SiO_{2-(140)}$ layer

c) Reference value (VPD, $1.5\times10^{12}$ P.cm$^{-2}$) was substracted

d) Reference value (SIMS, $1.2\times10^{12}$ P.cm$^{-2}$) was substracted

As previously studied with $SiO_2$ NPs, we assessed the capping properties of the POSS scaffold on POSS-P/wafers submitted or not to an oxidation step (500 °C, 2 h) prior to RTP at 1000 °C. When protected by the thin layer of $SiO_2$ generated *in-situ* by oxidation, phosphorus amounts of about $4.9 \times 10^{12}$ P atoms cm$^{-2}$ and $6.1 \times 10^{12}$ P atoms cm$^{-2}$ were found in $SiO_2$ and Si, respectively (Table 1). When protection was provided by the POSS cage itself, no major changes of phosphorus content were observed in silica ($2.2 \times 10^{12}$ P atoms cm$^{-2}$) and in silicon ($7.0 \times 10^{12}$ P atoms cm$^{-2}$), together with low carbon contamination (Figure S9). The two capping strategies ($O_2$ or $O_2$-free treatment) thus exhibit no significant differences in silicon doping efficiency.[59] Here, the dopant concentrations obtained in oxide-passivated silicon are in the same range of previously reported values (~$17 \times 10^{12}$ atoms cm$^{-2}$) when using MLD on H-terminated substrates.[17]

Finally, sheet resistance (Rs) measurements were performed to confirm the incorporation of electrically active impurities into the low-doped p-type Si substrate. After spike annealing (1000 °C, 1s), freshly cleaned $O_2$ and $O_2$-free treated samples, which contain comparable phosphorus doses, exhibit similar Rs values of about $8.5 \pm 0.3 \times 10^3$ Ω/□. These measured Rs are much lower than the resistance found for the control wafer (Rs ≥ $10^5$ Ω/□), and thus confirm the n-doping of Si through the use of **POSS-P**. Considering the doping levels reported here (~7

× $10^{12}$ P atoms $cm^{-2}$), Rs values are in the same order of magnitude than previously reported data obtained with mixed MLD,[55] spin-on doping[60] or MLCD.[29]

## CONCLUSIONS

We have shown that grafting a molecular phosphorus precursor bearing a POSS scaffold is as an efficient approach to dope thin oxide-passivated silicon. Detailed characterization of surface species generated on partially dehydroxylated $SiO_2$ nanoparticles used as model for the silica passivation layer of silicon wafers allowed us to ascertain (i) the structure of phosphorus-containing surface species formed by grafting the phosphorus precursor (POSS-P) on silica, and (ii) the role of the POSS scaffold in controlling the density of P atoms, and in favoring the diffusion of phosphorus into the silicon substrate in place of evaporation through self-capping. On wafers, submonolayer formation by the controlled grafting of POSS-P on a 0.7 nm silica layer and subsequent doping of silicon at 1000 °C by spike annealing under inert atmosphere yielded electrically active materials with doping level of ~7 × $10^{12}$ P atoms $cm^{-2}$. *In-situ* generation of a nano-layer of $SiO_2$ before annealing allows embedding P atoms and avoiding phosphorus volatilization for temperature below 800 °C, making this approach a suitable alternative to thick $SiO_2$ capping commonly used. These results open new perspectives for the design of dopant-containing molecular precursors with silica-like scaffold, suitable for manufacturing-friendly *n*- or *p*-doping processes.

## ACKNOWLEDGEMENT

The authors thank the transversal CEA project Zero POVA, CNRS and ERC Advanced Grant No. 320860 for funding, S. Deleonibus (DRT/LETI), M. Sanquer (DSM/INAC) and L. Vandroux (DRT/LETI) for their continuous support, as well as V. Loup, P. Besson, M.

Danielou, S. Kerdiles, A. André, L. Andreutti and J.P. Barnes from CEA/LETI/Minatec; and K. Szeto from C2P2-LCOMS. ETH Zürich, CPE Lyon and UCBL are also acknowledged for their scientific support and the access to the process and characterization facilities.

## ASSOCIATED CONTENT

**Supporting Information**. Experimental and computational details; *in-situ* IR and solid-state NMR spectra are available free of charge on the ACS Publications website.

## AUTHOR INFORMATION

Corresponding Author

*E-mail: ccoperet@inorg.chem.ethz.ch

*E-mail: thieuleux@cpe.fr

### Present Addresses

† Raphael Wischert:

Eco-Efficient Products and Processes Laboratory (E2P2L), UMI 3464 CNRS – Solvay, 3966 Jin Du Road, Xin Zhuang Ind. Zone, 201108 Shanghai, China.

### Author Contributions

The manuscript was written through contributions of all authors. All authors have given approval to the final version of the manuscript.

## REFERENCES

(1) Norris, D. J.; Efros, A. L.; Erwin, S. C. Doped Nanocrystals. *Science* **2008**, *319* (5871), 1776–1779.

(2) Erwin, S. C.; Zu, L.; Haftel, M. I.; Efros, A. L.; Kennedy, T. A.; Norris, D. J. Doping Semiconductor Nanocrystals. *Nature* **2005**, *436* (7047), 91–94.

(3) Bryan, J. D.; Gamelin, D. R. Doped Semiconductor Nanocrystals: Synthesis, Characterization, Physical Properties, and Applications. In *Progress in Inorganic Chemistry*; John Wiley & Sons, Inc., 2005; pp 47–126.
(4) Gandhi, R.; Zhixian, C.; Singh, N.; Banerjee, K.; Sungjoo, L. Vertical Si-Nanowire N-Type Tunneling FETs With Low Subthreshold Swing (<50mV/decade) at Room Temperature. *Electron Device Lett. IEEE* **2011**, *32* (4), 437–439.
(5) Thelander, C.; Agarwal, P.; Brongersma, S.; Eymery, J.; Feiner, L. F.; Forchel, A.; Scheffler, M.; Riess, W.; Ohlsson, B. J.; Gösele, U.; Samuelson, L. Nanowire-Based One-Dimensional Electronics. *Mater. Today* **2006**, *9* (10), 28–35.
(6) Czaban, J. A.; Thompson, D. A.; LaPierre, R. R. GaAs Core-Shell Nanowires for Photovoltaic Applications. *Nano Lett.* **2009**, *9* (1), 148–154.
(7) Yang, C.; Zhong, Z.; Lieber, C. M. Encoding Electronic Properties by Synthesis of Axial Modulation-Doped Silicon Nanowires. *Science* **2005**, *310* (5752), 1304–1307.
(8) Patolsky, F.; Zheng, G.; Hayden, O.; Lakadamyali, M.; Zhuang, X.; Lieber, C. M. Electrical Detection of Single Viruses. *Proc. Natl. Acad. Sci. U. S. A.* **2004**, *101* (39), 14017–14022.
(9) Garnett, E. C.; Brongersma, M. L.; Cui, Y.; McGehee, M. D. Nanowire Solar Cells. *Annu Rev Mater Res* **2001**, *41*, 269–295.
(10) International Technology Roadmap for Semiconductors 2011, Emerging Research Materials Section.
(11) Shinada, T.; Okamoto, S.; Kobayashi, T.; Ohdomari, I. Enhancing Semiconductor Device Performance Using Ordered Dopant Arrays. *Nature* **2005**, *437* (7062), 1128–1131.
(12) Beckman, R. A.; Johnston-Halperin, E.; Melosh, N. A.; Luo, Y.; Green, J. E.; Heath, J. R. Fabrication of Conducting Si Nanowire Arrays. *J. Appl. Phys.* **2004**, *96* (10), 5921–5923.
(13) Fuechsle, M.; Miwa, J. A.; Mahapatra, S.; Ryu, H.; Lee, S.; Warschkow, O.; Hollenberg, L. C. L.; Klimeck, G.; Simmons, M. Y. A Single-Atom Transistor. *Nat Nano* **2012**, *7* (4), 242–246.
(14) O'Connell, J.; Verni, G. A.; Gangnaik, A.; Shayesteh, M.; Long, B.; Georgiev, Y. M.; Petkov, N.; McGlacken, G. P.; Morris, M. A.; Duffy, R.; Holmes, J. D. Organo-Arsenic Molecular Layers on Silicon for High-Density Doping. *ACS Appl. Mater. Interfaces* **2015**, *7* (28), 15514–15521.
(15) Shimizu, Y.; Takamizawa, H.; Inoue, K.; Yano, F.; Nagai, Y.; Lamagna, L.; Mazzeo, G.; Perego, M.; Prati, E. Behavior of Phosphorous and Contaminants from Molecular Doping Combined with a Conventional Spike Annealing Method. *Nanoscale* **2014**, *6* (2), 706–710.
(16) Ang, K. W.; Barnett, J.; Loh, W. Y.; Huang, J.; Min, B. G.; Hung, P. Y.; Ok, I.; Yum, J. H.; Bersuker, G.; Rodgers, M.; Kaushik, V.; Gausepohl, S.; Hobbs, C.; Kirsch, P. D.; Jammy, R. 300mm FinFET Results Utilizing Conformal, Damage Free, Ultra Shallow Junctions (Xj~5nm) Formed with Molecular Monolayer Doping Technique. In *Electron Devices Meeting (IEDM), 2011 IEEE International*; 2011; pp 35.5.1–35.5.4.
(17) Ho, J. C.; Yerushalmi, R.; Smith, G.; Majhi, P.; Bennett, J.; Halim, J.; Faifer, V. N.; Javey, A. Wafer-Scale, Sub-5 Nm Junction Formation by Monolayer Doping and Conventional Spike Annealing. *Nano Lett* **2009**, *9*, 725–730.
(18) Ho, J. C.; Yerushalmi, R.; Jacobson, Z. A.; Fan, Z.; Alley, R. L.; Javey, A. Controlled Nanoscale Doping of Semiconductors via Molecular Monolayers. *Nat Mater* **2008**, *7*, 62–67.

(19) Buriak, J. M.; Sikder, M. D. H. From Molecules to Surfaces: Radical-Based Mechanisms of Si–S and Si–Se Bond Formation on Silicon. *J. Am. Chem. Soc.* **2015**, *137* (30), 9730–9738.
(20) Kachian, J. S.; Wong, K. T.; Bent, S. F. Periodic Trends in Organic Functionalization of Group IV Semiconductor Surfaces. *Acc. Chem. Res.* **2010**, *43* (2), 346–355.
(21) Buriak, J. M. Organometallic Chemistry on Silicon and Germanium Surfaces. *Chem. Rev.* **2002**, *102* (5), 1271–1308.
(22) Prasittichai, C.; Zhou, H.; Bent, S. F. Area Selective Molecular Layer Deposition of Polyurea Films. *ACS Appl. Mater. Interfaces* **2013**, *5* (24), 13391–13396.
(23) Loscutoff, P. W.; Lee, H.-B.-R.; Bent, S. F. Deposition of Ultrathin Polythiourea Films by Molecular Layer Deposition. *Chem. Mater.* **2010**, *22* (19), 5563–5569.
(24) Chen, R.; Bent, S. F. Highly Stable Monolayer Resists for Atomic Layer Deposition on Germanium and Silicon. *Chem. Mater.* **2006**, *18* (16), 3733–3741.
(25) Longo, R. C.; Mattson, E. C.; Vega, A.; Cabrera, W.; Cho, K.; Chabal, Y. J.; Thissen, P. Mechanism of Arsenic Monolayer Doping of Oxide-Free Si(111). *Chem. Mater.* **2016**, *28* (7), 1975–1979.
(26) Longo, R. C.; Cho, K.; Schmidt, W. G.; Chabal, Y. J.; Thissen, P. Monolayer Doping via Phosphonic Acid Grafting on Silicon: Microscopic Insight from Infrared Spectroscopy and Density Functional Theory Calculations. *Adv. Funct. Mater.* **2013**, *23* (27), 3471–3477.
(27) Vega, A.; Thissen, P.; Chabal, Y. J. Environment-Controlled Tethering by Aggregation and Growth of Phosphonic Acid Monolayers on Silicon Oxide. *Langmuir* **2012**, *28* (21), 8046–8051.
(28) Hazut, O.; Huang, B.-C.; Pantzer, A.; Amit, I.; Rosenwaks, Y.; Kohn, A.; Chang, C.-S.; Chiu, Y.-P.; Yerushalmi, R. Parallel P-N Junctions across Nanowires by One-Step Ex Situ Doping. *ACS Nano* **2014**, *8* (8), 8357–8362.
(29) Hazut, O.; Agarwala, A.; Amit, I.; Subramani, T.; Zaidiner, S.; Rosenwaks, Y.; Yerushalmi, R. Contact Doping of Silicon Wafers and Nanostructures with Phosphine Oxide Monolayers. *ACS Nano* **2012**, *6* (11), 10311–10318.
(30) Wegener, S. L.; Marks, T. J.; Stair, P. C. Design Strategies for the Molecular Level Synthesis of Supported Catalysts. *Acc. Chem. Res.* **2012**, *45* (2), 206–214.
(31) Tada, M.; Iwasawa, Y. *Supported Catalysts from Chemical Vapor Deposition and Related Techniques*; 2008.
(32) Copéret, C.; Chabanas, M.; Petroff Saint-Arroman, R.; Basset, J.-M. Homogeneous and Heterogeneous Catalysis: Bridging the Gap through Surface Organometallic Chemistry. *Angew. Chem. Int. Ed.* **2003**, *42* (2), 156–181.
(33) Thomas, J. M. Design, Synthesis, and In Situ Characterization of New Solid Catalysts. *Angew. Chem. Int. Ed.* **1999**, *38* (24), 3588–3628.
(34) Pujari, S. P.; Scheres, L.; Marcelis, A. T. M.; Zuilhof, H. Covalent Surface Modification of Oxide Surfaces. *Angew. Chem. Int. Ed.* **2014**, *53* (25), 6322–6356.
(35) Agarwala, A.; Subramani, T.; Goldbourt, A.; Danovich, D.; Yerushalmi, R. Facile Monolayer Formation on SiO2 Surfaces via Organoboron Functionalities. *Angew. Chem. Int. Ed.* **2013**, *52* (29), 7415–7418.
(36) Queffélec, C.; Petit, M.; Janvier, P.; Knight, D. A.; Bujoli, B. Surface Modification Using Phosphonic Acids and Esters. *Chem. Rev.* **2012**, *112* (7), 3777–3807.
(37) ter Maat, J.; Regeling, R.; Yang, M.; Mullings, M. N.; Bent, S. F.; Zuilhof, H. Photochemical Covalent Attachment of Alkene-Derived Monolayers onto Hydroxyl-Terminated Silica. *Langmuir* **2009**, *25* (19), 11592–11597.

(38) Yerushalmi, R.; Ho, J. C.; Fan, Z.; Javey, A. Phosphine Oxide Monolayers on SiO2 Surfaces. *Angew Chem Int Ed* **2008**, *47*, 4440–4442.
(39) Mathey, L.; Alphazan, T.; Valla, M.; Veyre, L.; Fontaine, H.; Enyedi, V.; Yckache, K.; Danielou, M.; Kerdiles, S.; Guerrero, J.; Barnes, J.-P.; Veillerot, M.; Chevalier, N.; Mariolle, D.; Bertin, F.; Durand, C.; Berthe, M.; Dendooven, J.; Martin, F.; Thieuleux, C.; Grandidier, B.; Copéret, C. Functionalization of Silica Nanoparticles and Native Silicon Oxide with Tailored Boron-Molecular Precursors for Efficient and Predictive P-Doping of Silicon. *J. Phys. Chem. C* **2015**, *119* (24), 13750–13757.
(40) Roussey, A.; Gentile, P.; Lafond, D.; Martinez, E.; Jousseaume, V.; Thieuleux, C.; Coperet, C. Cu Nanoparticles on 2D and 3D Silica Substrates: Controlled Size and Density, and Critical Size in Catalytic Silicon Nanowire Growth. *J. Mater. Chem. C* **2013**, *1* (8), 1583–1587.
(41) Thissen, P.; Vega, A.; Peixoto, T.; Chabal, Y. J. Controlled, Low-Coverage Metal Oxide Activation of Silicon for Organic Functionalization: Unraveling the Phosphonate Bond. *Langmuir* **2012**, *28* (50), 17494–17505.
(42) Hanson, E. L.; Schwartz, J.; Nickel, B.; Koch, N.; Danisman, M. F. Bonding Self-Assembled, Compact Organophosphonate Monolayers to the Native Oxide Surface of Silicon. *J. Am. Chem. Soc.* **2003**, *125* (51), 16074–16080.
(43) Feher, F. J.; Budzichowski, T. A. Heterosilsesquioxanes: Synthesis and Characterization of Group 15 Containing Polyhedral Oligosilsesquioxanes. *Organometallics* **1991**, *10* (3), 812–815.
(44) Cordes, D. B.; Lickiss, P. D.; Rataboul, F. Recent Developments in the Chemistry of Cubic Polyhedral Oligosilsesquioxanes. *Chem. Rev.* **2010**, *110* (4), 2081–2173.
(45) Rossini, A. J.; Zagdoun, A.; Lelli, M.; Lesage, A.; Copéret, C.; Emsley, L. Dynamic Nuclear Polarization Surface Enhanced NMR Spectroscopy. *Acc. Chem. Res.* **2013**, *46* (9), 1942–1951.
(46) Lelli, M.; Gajan, D.; Lesage, A.; Caporini, M. A.; Vitzthum, V.; Miéville, P.; Héroguel, F.; Rascón, F.; Roussey, A.; Thieuleux, C.; Boualleg, M.; Veyre, L.; Bodenhausen, G.; Coperet, C.; Emsley, L. Fast Characterization of Functionalized Silica Materials by Silicon-29 Surface-Enhanced NMR Spectroscopy Using Dynamic Nuclear Polarization. *J. Am. Chem. Soc.* **2011**, *133* (7), 2104–2107.
(47) Lesage, A.; Lelli, M.; Gajan, D.; Caporini, M. A.; Vitzthum, V.; Miéville, P.; Alauzun, J.; Roussey, A.; Thieuleux, C.; Mehdi, A.; Bodenhausen, G.; Coperet, C.; Emsley, L. Surface Enhanced NMR Spectroscopy by Dynamic Nuclear Polarization. *J. Am. Chem. Soc.* **2010**, *132* (44), 15459–15461.
(48) Shabani, M. B.; Shiina, Y.; Kirscht, F. G.; Shimanuki, Y. Recent Advanced Applications of AAS and ICP-MS in the Semiconductor Industry. *Mater. Sci. Eng. B* **2003**, *102* (1-3), 238–246.
(49) Jones Ferrero, E.; Posey, D. Improving the Detection Limits for Vapor Phase Decomposition-Inductively Coupled Plasma Mass Spectrometry (VPD-ICP-MS) Analysis. *J. Anal. At. Spectrom.* **2002**, *17* (9), 1194–1201.
(50) Tan, S. H. Application of Vapor Phase Decomposition Techniques (VPD/AAS and ICP-MS) for Trace Element Analysis in Oxide Coatings on Silicon. *Nucl. Instrum. Methods Phys. Res. Sect. B Beam Interact. Mater. At.* **1995**, *99* (1-4), 458–461.
(51) Copéret, C.; Comas-Vives, A.; Conley, M. P.; Estes, D. P.; Fedorov, A.; Mougel, V.; Nagae, H.; Núñez-Zarur, F.; Zhizhko, P. A. Surface Organometallic and Coordination Chemistry toward Single-Site Heterogeneous Catalysts: Strategies, Methods, Structures, and Activities. *Chem. Rev.* **2016**, A – CU.

(52) Gay, I. D.; McFarlan, A. J.; Morrow, B. A. Trimethyl Phosphite Adsorbed on Silica: An NMR and Infrared Study. *J. Phys. Chem.* **1991**, *95* (3), 1360–1368.
(53) Vicente, B. C.; Huang, Z.; Brookhart, M.; Goldman, A. S.; Scott, S. L. Reactions of Phosphinites with Oxide Surfaces: A New Method for Anchoring Organic and Organometallic Complexes. *Dalton Trans.* *40* (16), 4268–4274.
(54) Morrow, B. A.; Lang, S. J.; Gay, I. D. An Infrared and 31P Magic Angle Spinning Nuclear Magnetic Resonance Study of the Adsorption of PCl3 and OPCl3 on Silica. *Langmuir* **1994**, *10* (3), 756–760.
(55) Ye, L.; Pujari, S. P.; Zuilhof, H.; Kudernac, T.; de Jong, M. P.; van der Wiel, W. G.; Huskens, J. Controlling the Dopant Dose in Silicon by Mixed-Monolayer Doping. *ACS Appl. Mater. Interfaces* **2015**, *7* (5), 3231–3236.
(56) Thissen, P.; Peixoto, T.; Longo, R. C.; Peng, W.; Schmidt, W. G.; Cho, K.; Chabal, Y. J. *J Am Chem Soc 134*, 8869.
(57) Kownacki, I.; Marciniec, B.; Szubert, K.; Kubicki, M.; Jankowska, M.; Steinberger, H.; Rubinsztajn, Si. Tris(triorganosilyl)phosphites—New Ligands Controlling Catalytic Activity of Pt(0) Complex in Curing of Silicone Rubber. *Appl. Catal. Gen.* **2012**, *380* (1-2), 105–112.
(58) Fina, A.; Tabuani, D.; Carniato, F.; Frache, A.; Boccaleri, E.; Camino, G. Polyhedral Oligomeric Silsesquioxanes (POSS) Thermal Degradation. *Thermochim. Acta* **2006**, *440* (1), 36–42.
(59) SIMS Analysis Performed after Annealing SiO2/Si Wafers Supported Phosphonate (1000°C, 1s) and Phosphonium (~1050°C, 1s) Species Revealed P Depth Profiles Very close to Control Sample, with Low Signal/noise Ratio. Silicon Doping Was Thus Considered Unsuccessful with These Two Molecular Compounds.
(60) Hoarfrost, M. L.; Takei, K.; Ho, V.; Heitsch, A.; Trefonas, P.; Javey, A.; Segalman, R. A. Spin-On Organic Polymer Dopants for Silicon. *J. Phys. Chem. Lett.* **2013**, *4* (21), 3741–3746.

## TOC

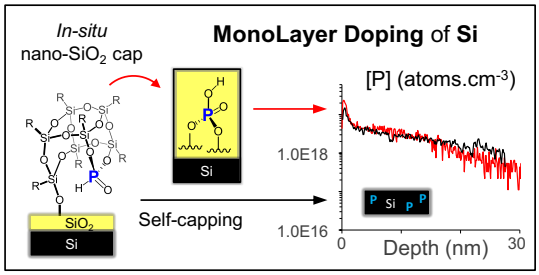

# Supporting Information

## Monolayer Doping of Silicon through Grafting a Tailored Molecular Phosphorus Precursor onto Oxide-Passivated Silicon Surfaces

*Thibault Alphazan,[†,‡,§] Laurent Mathey,[†,‡,§] Martin Schwarzwälder,[‖] Tsung-Han Lin,[‖] Aaron J. Rossini,[#] Raphaël Wischert,[‖] Virginie Enyedi,[†,‡] Hervé Fontaine,[†,‡] Marc Veillerot,[†,‡] Anne Lesage,[⊽] Lyndon Emsley,[#] Laurent Veyre,[§] François Martin,[†,‡] Chloé Thieuleux,[§,]* and Christophe Copéret[‖]**

[†] Univ. Grenoble Alpes, F-38000 Grenoble, France.

[‡] CEA, LETI, MINATEC Campus, F-38054 Grenoble, France.

[§] C2P2, CPE Lyon, 43 Bd du 11 Nov. 1918, 69616 Villeurbanne cedex France

[‖] ETH Zürich, Department of Chemistry and Applied Biosciences, Vladimir Prelog Weg. 1-5, CH-8093 Zürich, Switzerland

[#] Institut des Sciences et Ingénierie Chimiques, Ecole Polytechnique Fédérale de Lausanne (EPFL), CH-1015 Lausanne, Switzerland

[⊽] Centre de RMN à Très Hauts Champs, Institut de Sciences Analytiques (CNRS/ENS Lyon/UCB Lyon

* C. Copéret: ccoperet@inorg.chem.ethz.ch

* C. Thieuleux: thieuleux@cpe.fr

# OUTLINE

## **SI 1.** General procedures and Methods

### Experimental

*Samples preparation.* All experiments, otherwise stated, were carried out under dry and oxygen free Ar atmosphere using either standard Schlenk or glovebox techniques for the organic synthesis. For syntheses and treatments of surface species, reactions were carried out using high vacuum lines ($10^{-5}$ mbar). Elemental analyses were performed at "Mikroanalytisches Labor Pascher" in Germany. Toluene, and pentane were dried using an MBraun solvent purification system, contacted with molecular sieves 4 Å and degassed under vacuum. Hepta-isobutyl-POSS triol (POSS-OH), phosphorus trichloride ($PCl_3$), diethyl-benzyl phosphonate (DEBP), ethyl-tosylate and triethylamine ($Et_3N$) were purchased from Sigma Aldrich. $PCl_3$ and $Et_3N$ were distilled prior to use. The $SiO_2$/Si wafers were 30 cm in diameter, *p*-doped ($10^{15}$ B.cm$^{-3}$) and double-face polished. Wafers with native oxide (~1.5 nm) were used as received. Chemical oxides (~0.7 or ~0.9 nm) were grown on silicon wafers in a SU-3100 from DNS, in clean rooms of LETI, CEA Grenoble. RTP and ICP-MS analyses on wafers were also performed in clean rooms (CEA Grenoble). RTP annealing experiments were done in a JetFirst 200 (Jipelec) using BT or HT type optical pyrometer and 2 K type (Chromel/Alumel) Ø 0.127 mm thermocouples.

*Conventional NMR experiments.* Liquid-state NMR spectra were recorded using a Bruker Spectrospin 300 MHz spectrometer. For *conventional solid-state NMR,* 40 to 50 mg of material was packed in 4.0 mm zirconia NMR rotor under inert atmosphere. NMR spectra were acquired either on a 300 MHz ($^{29}$Si) or 500 MHz ($^{1}$H/$^{13}$C/$^{31}$P) ultrashielded Bruker NMR spectrometer. $^{1}$H, $^{13}$C, $^{31}$P and $^{29}$Si spectra were recorded using a 4.0 mm cross-polarization (CP) magic angle spinning (MAS) probe with a sample temperature of 294 K and sample spinning frequencies between 5 to 10 kHz. Standard CP was used to record $^{29}$Si and $^{13}$C spectra.

*DNP SENS experiments.* 12.5 to 14.7 mg of material was wetted with 20 to 25 µl of a solution of 16 mM TEKPol in 1,1,2,2-tetrachloroethane. The impregnated powder was then packed into a 3.2 mm NMR rotor, under air. A sapphire NMR rotor was used to maximize microwave penetration throughout the sample. The rotor was capped with a zirconia drive cap and quickly inserted into the DNP spectrometer. Several insert and eject cycles were performed to guarantee good glass quality as well as de-oxygenation of the sample. All spectra were acquired on a Bruker Avance I or Avance III 400 MHz DNP NMR spectrometer equipped with a 263 GHz gyrotron microwave system ($B_0$ = 9.4 T, $\omega_H/2\pi$ = 400 MHz, $\omega_P/2\pi$ = 162.0 MHz).[1] The field sweep coil of the NMR magnet was set so that MW irradiation occurred at the DNP enhancement maximum of TOTAPOL, with an estimated 8 W power of the MW beam at the output of the probe waveguide. $^{1}$H and $^{31}$P DNP-SENS spectra were recorded using a triple resonance low-temperature CPMAS probe with a sample temperature of 105 K and sample spinning frequencies between 8 to 12.5 kHz. SPINAL-64 heteronuclear decoupling[2] was applied during acquisition ($\omega_H/2\pi$ = 100 kHz). Standard CP was used for $^{31}$P spectra where SPINAL-64 proton decoupling was applied during the acquisition. Processing of the spectra and fitting of the chemical shift anisotropy (CSA) parameters was done using the Topspin software package. $^{1}$H, $^{13}$C and chemical shifts are referenced to TMS at 0 ppm.

*Ellipsometric measurements.* The $SiO_2$/Si model used to fit ellipsometric data (Figure S1-a) was considered to be a relevant model for the POSS-P, which contains a silica-like scaffold. Comparison of the very good fits obtained for reference and grafted samples shows an increase of about 1.0 (±0.2) nm of thickness after deposition of POSS-P. Such an increase of thickness is similar to the calculated projected radius of POSS-P (~ 0.8 nm), and is consistent with monolayer formation previously reported for other B- or P-species:[3,4] we thus assumed that a monolayer of surface species was formed after grafting POSS-P.

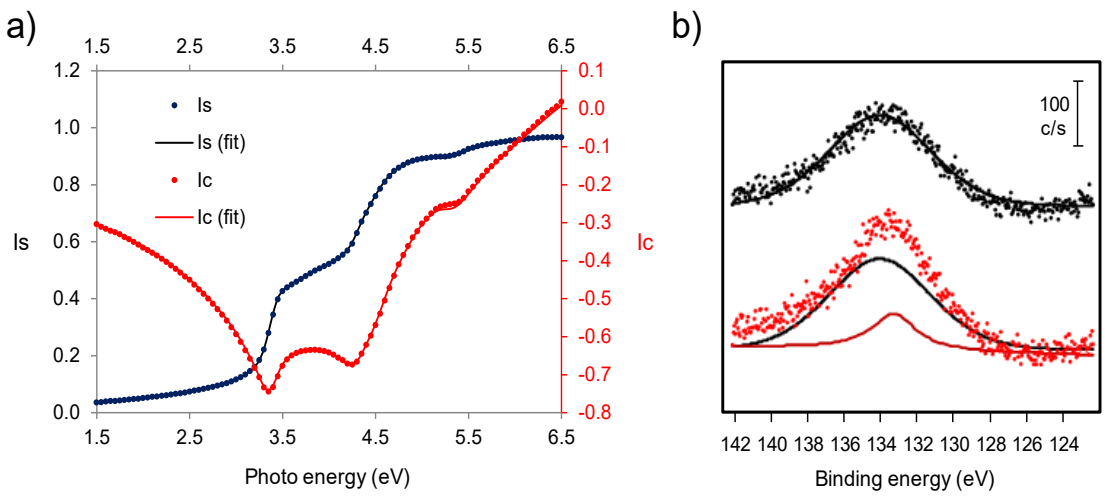


**Figure S1.** (a) Ellipsometric data (dots) and corresponding fit (lines), obtained for POSS-P/$SiO_2$/Si wafer, (b) XPS analysis with P 2p region before (black dots) and after (red dots) grafting POSS-P onto $SiO_2$/Si.

*XPS analysis.* XPS spectra were recorded on a VersaProbe II spectrometer from Physical Electronics equipped with a 180° hemispherical electron energy analyzer, and using a high-resolution monochromatic Al-Kα line X-ray source at 1486.7 eV. A pass energy of 23 eV was used for core level analysis leading to an overall energy resolution of 0.6 eV. The photoelectron take-off angle was 45°, yielding an integrated sampling depth of approximately 5 nm. Measurements were made at ambient temperature, at a pressure lower than $10^{-8}$ Pa in the analysis chamber. All spectra were referenced against the C 1s level peak at a binding energy of 284.8 eV. The spectra were analyzed using the CASA XPS software. XPS samples were prepared as follows: SiO2/Si $wafer_{-(140)}$ were immersed into a 80 µM pentane solution of POSS-P under argon, and the temperature was raised to 30°C until pentane evaporation, giving POSS-P adsorbed onto $wafer_{-(140)}$. Subsequent rinsing with pentane removed physisorbed species and led to chemisorbed POSS-P/$wafer_{-(140)}$.

Figure S1-b. shows P 2p region of POSS-P/$SiO_2$/Si (red dots) and $SiO_2$/Si (black dots) samples. The broad plasmon loss peak of silicon centered at 134 eV is visible on the black spectrum (black line), and partly overlaps the P 2p photopeak of P species on the red spectrum which is highlighted by the red line. An unresolved P $2p_{3/2}$,$2p_{3/2}$ photopeak centered at ~133.3 eV is thus observed (red solid line), and is assigned to P(V) species,[4] chemisorbed on the substrate.[4–6]

*Other analyses:* An Agilent ICP-MS-MS 8800 was used for the ICP-MS measurements with the following parameters: analysis hot plasma mode (1500W), $O_2$ as reacting gas (mass 31 (P) on detector n°1, mass 47 (P + $O_2$) on detector n°2). Time of flight SIMS analyses were performed on a TOF SIMS 5 instrument from IONTOF. FTIR spectra recorded in diffuse reflectance infrared Fourier transform spectroscopy (DRIFT) mode were obtained on a Nicolet 6700 FT-IR spectrometer equipped with a HgCdTe (MCT) detector cooled with liquid $N_2$. The samples were loaded into a custom DRIFT cell equipped with $CaF_2$ windows under inert atmosphere (glovebox). Typically, 32 to 64 scans were acquired (4 $cm^{-1}$ resolution).

*Synthesis of hepta-isobutyl-polyhedral oligomeric silsesquioxane phosphorus triester (**POSS-P**)*. In a schlenk was prepared a 20 mL-toluene solution of POSS-OH (1.159 g, 1.46 mmol) and $Et_3N$ (0.730 mL, 3.3 eq.) under gentle stirring. A 10 mL-toluene solution of $PCl_3$ (0.145 ml, 1.60 mmol, 1.1 eq.) was then added dropwise over 10 min. A white slurry immediately appeared, and the solution was left to react for 2 h. Volatiles were removed *in vacuo*, and the remaining solid was suspended in pentane and filtrated over Celite®. Recrystallisation of the resulting solution (-30 °C, overnight) yielded crystals collected in two crops, which were dried under vacuum to give pure **POSS-P** as a white powder. Yield: 34% (0.411 g). **$^1$H NMR** ($C_6D_6$, 25 °C, ppm): $\delta_H$= 2.1 (m, 1H, $CH_2CH(CH_3)_2$), 1.1 (d, 6H, $CH_2CH(CH_3)_2$), 0.8 (d, 2H, $CH_2CH(CH_3)_2$). **$^{13}$C NMR** (ppm): $\delta_C$= 25.9 (2C, $CH_2CH(CH_3)_2$), 24.3 (1C, $CH_2CH(CH_3)_2$), 23.0 (1C, $CH_2CH(CH_3)_2$). **$^{29}$Si NMR** (ppm): $\delta_{Si}$= –66.3 (3Si, *Si*-O-P), –67.4, –67.5, –70.5, –71.1 (4Si, *Si*-O-Si*)*.**$^{31}$P NMR** (ppm): $\delta_P$= 84.7.

*Synthesis of tosylate tributyl-ethylphosphonium (**TBEP**).* In a 100 mL Schlenk flask blown with argon, 12.223 g of ethyl-tosylate (61.0 mmol) were diluted in 44 mL of toluene. Then, 14 mL of tributylphosphine (11.3 g; 56.1 mmol, 0.9 eq) were added to the solution. A water cooler was adapted to the flask and the mixture was heated up and left to be stirred at 90 °C overnight (12 h). All volatiles were then taken *in vacuo*. The flask was cooled down to RT (24 °C) and the resulting white solid was then suspended in dry diethyl ether and filtered. The product was heated up to 90°C and melted down, and all volatiles were taken *in vacuo*. The flask was again allowed to cool down to RT (24 °C) and stored in the glovebox. **$^1$H NMR** ($CDCl_3$, 25 °C, ppm): $\delta_H$= 0.97 (m, 9H, $CH_2CH_2CH_2CH_3$), 1.28 ppm (m, 3H, $CH_2CH_3$), 1.52 ppm (large peak, 8H, $CH_2CH_2CH_2CH_3$ and $CH_2CH_3$), 2.34 ppm (s;3H; $CH_{3\_Tos}$), 2.45 (m, 12H, $CH_2CH_2CH_2CH_3$); 7.14 ppm (d, 10 Hz, 2H, $H_{Ar\_Tos}$), 7.81 ppm (d; 10 Hz; 2H, $H_{Ar\_Tos}$). **$^{31}$P NMR** (ppm): $\delta_P$= 34.6.

**Study on silica nanoparticles (NPs).**

*Preparation of partially dehydroxylated silica at 700 °C ($SiO_{2-(700)}$). Representative procedure*. Silica (Aerosil Degussa, 200 $m^2.g^{-1}$) was compacted using distilled water and dried at 110°C for 5 days in an oven. The obtained compacted solids were broken down in a mortar and sieved to yield agglomerates of about 50 meshes (particles of ca. Ø ≈ 20 nm). The thus-obtained powder was calcined for 5 h under air at 500 °C (6 $°C.min^{-1}$), partially dehydroxylated at 500°C in secondary vacuum ($10^{-5}$ mbar) for 12 h, then at 700 °C for 10 h, and finally stored in the glovebox. $\mathbf{S_{BET}}$ ($m^2.g^{-1}$): 197. **IR** ($cm^{-1}$): 3747 (isolated SiOH), 3600 (large peak, very low intensity, bonded SiOH).

*Preparation of partially dehydroxylated silica at 500 °C ($SiO_{2-(500)}$). $SiO_{2-(500)}$* was prepared according to the representative procedure. $\mathbf{S_{BET}}$ ($m^2.g^{-1}$): 198. **IR** ($cm^{-1}$): 3745 (isolated SiOH), 3600 (large peak, low intensity, bonded SiOH).

*Preparation of silica dehydrated at 140 °C ($SiO_{2-(140)}$).* Silica powder was loaded in a reactor, put under secondary vacuum ($10^{-5}$ mbar) and heated up to 140 °C for 17 h, and stored in the glovebox. $\mathbf{S_{BET}}$ ($m^2.g^{-1}$): 196. **IR** ($cm^{-1}$): 3741 (isolated SiOH), 3660 & 3540 (large peaks, medium intensity, bonded SiOH).

*Dosing SiOH groups on $SiO_{2-(140)}$. Representative procedure.* A small Schlenk was loaded with $SiO_{2-(140)}$ (267.4 mg) and equipped with a pressure equalizing dropping funnel loaded with ~2 ml of pentane. About 1.0 ml of BuMgCl•$Et_2O$ was added, mixed with pentane and slowly added onto silica. After 30 min under gentle stirring, the gas phase was transferred to an expansion flask (6678 ml). After 16 h, the gas phase (300 µl) was analyzed by GC (KCl alumina column, 40°C (isotherm), injector 280°C). Results (~4.6 OH/nm²) were averaged on 3 measurements.

*Grafting of POSS-P on $SiO_{2-(500)}$*. Representative procedure.

POSS-P (244 mg, 3.0 x $10^{-4}$ mol) was solubilized in pentane (10 mL) and was subsequently contacted with $SiO_{2-(500)}$ (488 mg, ~3.2 x $10^{-4}$ mol surface silanol) at 25 °C for 2.5 h, under gentle stirring. After filtration, the solid was washed 3 times with pentane, and all volatile compounds were removed *in vacuo*. The resulting solid **POSS-P/$SiO_{2-(500)}$** was dried under high vacuum ($10^{-5}$ mbar) and the grafted species were then stored under Argon. **IR** ($cm^{-1}$): 3745 (weak, remaining isolated SiOH), 3703 (perturbed, H-bonded SiOH), 3326 (broad), 2960, 2934, 2909 & 2876 (ν(C-H)), 2450 & 2425 (ν(P-H)), 1468 (δ(C-H)). **$^{1}$H NMR** (ppm): $\delta_H$= 6.9 (d, very weak, *H*-P, $J_{PH}$~700 Hz), 1.9 ($CH_2CH(CH_3)_2$), 0.9 ($CH_2CH(CH_3)_2$ and $CH_2CH(CH_3)_2$). **$^{13}$C NMR** (CP-MAS, ppm): $\delta_C$= 23 (broad). **$^{31}$P NMR** (HP-Dec, ppm): $\delta_P$= –19; –26 (sh). **$^{29}$Si NMR** (CP-MAS, ppm): $\delta_{Si}$= –66 ($T_3$-type Si, POSS cage), 92, 101 & 110 (Q-type Si, $SiO_2$ network). **Elemental analysis**: 4.85 wt % C, 0.91 wt % H, 0.47 wt % P, 42.4 wt % Si, *i.e.* H/C(at/at)= 2.3 (th. 2.3), C/P= 26.7 (th 28.0) and P/Si (×100)= 1.00.

*Grafting of POSS-P on $SiO_{2-(700)}$*. **POSS-P/$SiO_{2-(700)}$** was prepared according to the representative procedure, with 264 mg of $SiO_{2-(700)}$ (~6.1 × $10^{-5}$ mol surface silanols) and 52 mg of POSS-P (6.5 × $10^{-5}$ mol). **IR** ($cm^{-1}$): 3746 (remaining isolated SiOH), 3715 (perturbed, H-bonded SiOH), 3250 (broad), 2958, 2938, 2909 & 2877 (ν(C-H)), 2450 & 2425 (ν(P-H)), 1468 (δ(C-H)). **$^{31}$P CP-MAS DNP-SENS** (ppm): $\delta_P$= –3, –16. **Elemental analysis**: 0.76 wt % P.

*Grafting of POSS-P on $SiO_{2-(140)}$*. **POSS-P/$SiO_{2-(140)}$** was prepared according to the representative procedure, with 312 mg of $SiO_{2-(140)}$ and 225 mg of POSS-P (2.7 × $10^{-4}$ mol). **IR** ($cm^{-1}$): 3690 (perturbed, H-bonded SiOH), 3430 (broad), 2960, 2934, 2909 & 2876 (ν(C-H)), 2450 & 2425 (ν(P-H)), 1468 δ(C-H). **$^{1}$H NMR** (ppm): $\delta_H$= 2.0 (-$CH_2CH(CH_3)_2$), 0.9 (-$CH_2CH(CH_3)_2$ and -$CH_2CH(CH_3)_2$). **$^{13}$C NMR** (CP-MAS, ppm): $\delta_C$= 23. **$^{31}$P NMR** (HP-Dec, ppm): $\delta_P$= –19, –26 (sh). **$^{29}$Si NMR** (CP-MAS, ppm): $\delta_{Si}$= –66 ($T_3$-type Si, POSS cage), 92, 101 & 110 (Q-type Si, $SiO_2$ network). **Elemental analysis**: 0.59 wt % P.

*Grafting of diethyl-benzyl phosphonate (**DEBP**) on $SiO_{2-(700)}$.* **DEBP/$SiO_{2-(700)}$** was prepared according to the representative procedure, with 567 mg of $SiO_{2-(700)}$ (~0.13 × $10^{-3}$ mol surface silanols) and ~37 mg of DEBP (~0.16 × $10^{-3}$ mol). **IR** ($cm^{-1}$): 3744 (remaining isolated SiOH), 3625 (perturbed, H-bonded SiOH), 3158 (broad), 3092, 3069 & 3036 v($Csp_2$-H), 2986, 2938, 2915, 2878 v($Csp_3$-H), 1605 & 1588 (δ($Csp_2$-H)), 1497 (δ($Csp_3$-H)). **Elemental analysis**: 4.57 wt % C, 1.04 wt % P.

*Adsorption of p-tosylate tributyl-ethylphosphonium (**TBEP**) on $SiO_{2-(700)}$.* **TBEP/$SiO_{2-(700)}$** was prepared according to the representative procedure, with 310 mg of $SiO_{2-(700)}$ (~6.6 × $10^{-5}$ mol surface silanols) and ~34 mg of TBEP (~0.16 × $10^{-3}$ mol). **IR** ($cm^{-1}$): 3745 (remaining isolated SiOH), 3150 (broad), 2967, 2932, 2912, 2877 v(C-H). **Elemental analysis**: 5.61 wt % C, 0.68 wt % S, 0.65 wt % P.

*Thermal treatment of **POSS-P/$SiO_{2-(500)}$** under air (oxidative atmosphere):* 340 mg of **POSS-P/$SiO_{2-(500)}$** were loaded in a quartz reactor and calcined at 500 °C under a flow of dry air (temperature ramp: 6 °C.$min^{-1}$, air flow: 50 mL.$min^{-1}$). **IR** ($cm^{-1}$): 3746 (isolated SiOH), 3671 v(P-OH). **$^{31}$P NMR** (HPDec, ppm): $\delta_P$= –24, –37. **$^{29}$Si NMR** (CP-MAS, ppm): $\delta_{Si}$= 92, 101 & 110 (Q-type Si, $SiO_2$ network). **Elemental analysis**: 0.13 wt % C; 0.14 wt % H; 0.48 wt % P, 44.0 wt % Si, *i.e.* C/P(at/at)= 0.7 and P/Si (×100)= 0.99.

*Thermal treatment of **POSS-P/$SiO_{2-(500)}$** under argon (inert conditions):* 310 mg of **POSS-P/$SiO_{2-(500)}$** were loaded in a quartz reactor and calcined at 500 °C under a flow of argon (temperature ramp: 6 °C.$min^{-1}$, argon flow: ~50 mL.$min^{-1}$). **IR** ($cm^{-1}$): 3704, 3316, 2960, 2934, 2909, 2876, 2460 (v(P-H)), 2250 (v(Si-H)), 1468 (v(C-H)). **$^{31}$P NMR** (HP-Dec, ppm): $\delta_P$= 108 (8%), –19 (92%). **$^{29}$Si NMR** (CP-MAS, ppm): $\delta_{Si}$= –57 ($T_2$-type Si-OH, POSS cage), –66 ($T_3$-type Si, POSS cage), 92, 101 & 110 (Q-type Si, $SiO_2$ network). **Elemental analysis**: 4.64 wt % C; 0.86 wt % H; 0.48 wt % P, 41.3 wt % Si, *i.e.* C/P(at/at)= 25.0 and P/Si (×100)= 1.05.

*Thermal treatment of* ***DEBP/SiO$_{2-(700)}$*** *under air (oxidative atmosphere):* 200 mg of **DEBP/SiO$_{2-(700)}$** were loaded in a quartz reactor and calcined at 500 °C under a flow of dry air (temperature ramp: 6 °C.min$^{-1}$, air flow: 50 mL.min$^{-1}$). **IR** (cm$^{-1}$): 3746 (isolated SiOH), 3671 ν(P-OH). **Elemental analysis**: 0.16 wt % C; 0.14 wt % P.

*Thermal treatment of* ***TBEP/SiO$_{2-(700)}$*** *under air (oxidative atmosphere):* 310 mg of **TBEP/SiO$_{2-(700)}$** were loaded in a quartz reactor and calcined at 500 °C under a flow of dry air (temperature ramp: 6 °C.min$^{-1}$, air flow: 50 mL.min$^{-1}$). **IR** (cm$^{-1}$): 3746 (isolated SiOH), 3671 ν(P-OH). **Elemental analysis**: 0.44 wt % C; 0.25 wt % P.

**Surface chemistry on wafers.**

*Grafting of POSS-P on wafers*. In the glovebox, a toluene or pentane solution of **POSS-P** (~80 μM) was prepared by solubilizing the POSS-P compound into 45 mL of solvent at 25 °C. Then, the wafer pieces (2.5×8 cm²) were immersed into the solution and left to react for 2 hours. The wafer pieces were then washed 3 times with toluene (5 mL) and/or with pentane (5 mL) before being dried *in vacuo*.

*Preparation of "control" wafers*. A wafer pieces was dipped in the neat solvent (45 mL) for 2 hours. Then, the solution was removed and all volatiles were removed *in vacuo* before putting the sample inside the glovebox. Finally, the wafer was annealed in the same conditions as its corresponding P-grafted counterpart.

## **SI 2.** DFT calculations

**Details of the calculations.** The *tert*-butyl groups on P-POSS were replaced with methyl groups in the calculations. All structures used for the NMR calculations were optimized with the B3-LYP hybrid density functional, as implemented in Gaussian 09 (Revision C.01).[7] The IGLO-II basis set[8] was used on all atoms. NMR shielding tensors were computed at the same level, using the Gauge-Independent Atomic Orbital (GIAO) method. The experimental $^{31}P$ chemical shifts are referenced to aqueous $H_3PO_4$, which is not easily described by computational methods. Therefore, following recommendation from others,[9,10] all chemical shifts (δ) were referenced to gaseous $PH_3$, using the experimental value *vs.* $H_3PO_4$ ($\delta_{exp}(PH_3) = -266.1$ ppm) as follows:

$$\delta_{calc} = \sigma_{calc}(PH_3) - \sigma_{calc} - \delta_{exp}(PH_3).$$

The isotropic chemical shift ($\delta_{iso}$), the span (Ω), and the skew (κ) were calculated according to the Herzfeld-Berger[11] convention:

$$\delta_{iso} = (\delta_{11} + \delta_{22} + \delta_{33})/3$$

$$\Omega = \delta_{11} - \delta_{33}$$

$$\kappa = 3(\delta_{22} - \delta_{iso})/\Omega$$

Harmonic vibrational frequencies were calculated at the B3-LYP/6-31G(d) level and scaled by a factor of 0.96.[12]

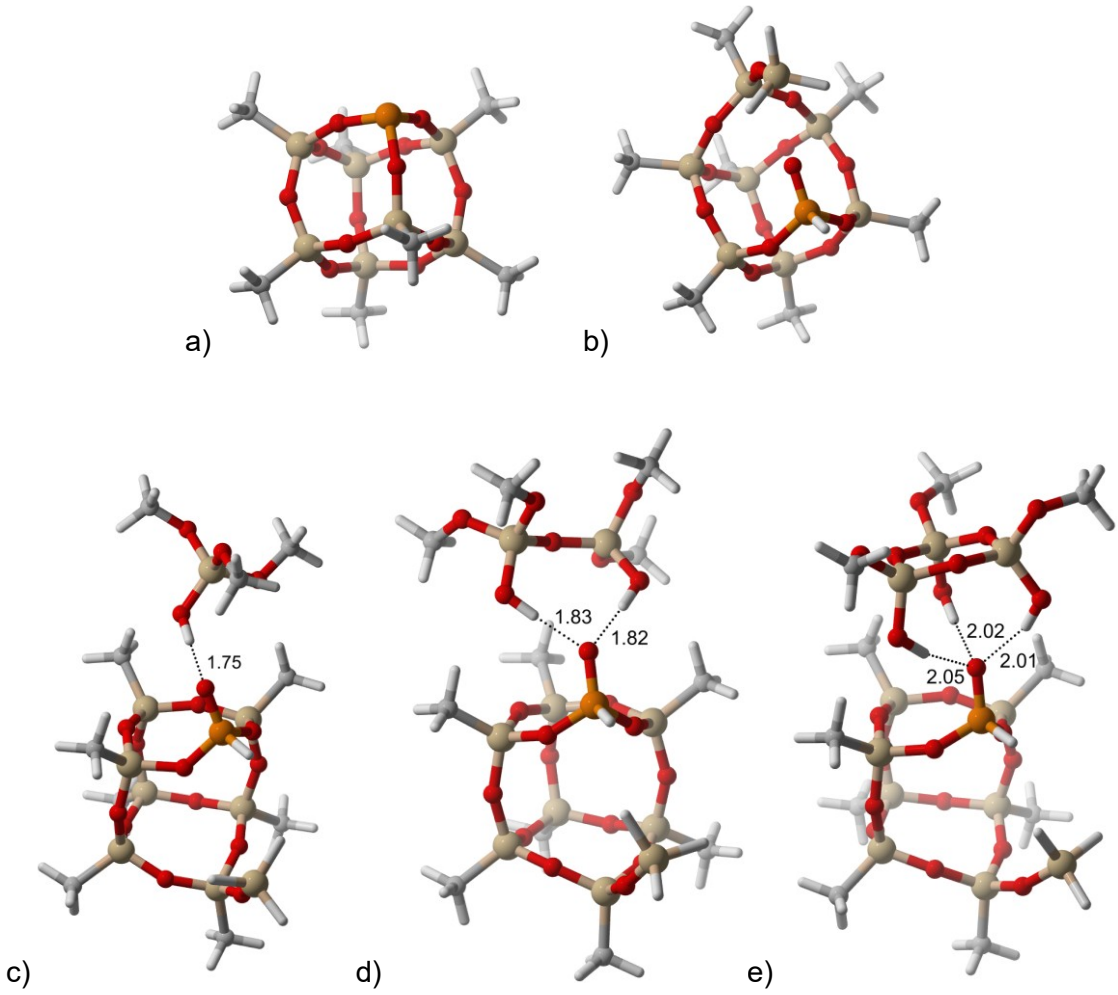


**Figure S2.** Optimized structures of a) P-POSS, b) POSS-Phosphonate, c) POSS-Phosphonate-silanol, d) POSS-Phosphonate-bis-silanol, e) POSS-Phosphonate-tris-silanol. Distances are given in Å.The figures were produced with the free Cylview software (CYLview, 1.0b; Legault, C. Y., Université de Sherbrooke, 2009 (http://www.cylview.org).

**Table S1.** Eigenvalues of the GIAO magnetic shielding tensor ($\sigma_{11}$, $\sigma_{22}$ and $\sigma_{33}$, in ppm), and corresponding isotropic shielding values ($\sigma_{iso}$, ppm) as calculated with Gaussian.

| | $\sigma_{11}$ | $\sigma_{22}$ | $\sigma_{33}$ | $\sigma_{iso}$ |
|---|---|---|---|---|
| $PH_3$ | 529.6623 | 587.267 | 587.3099 | 568.1 |
| POSS-Me terminated | 142.955 | 143.5882 | 402.3732 | 229.6 |
| POSS-Phosphonate | 236.7698 | 280.1999 | 498.3533 | 338.4 |
| POSS-Phosphonate-silanol | 242.0736 | 285.9143 | 461.2441 | 329.7 |
| POSS-Phosphonate-bis-silanol | 251.108 | 291.9551 | 448.1499 | 330.4 |
| POSS-Phosphonate-tris-silanol | 246.9235 | 294.996 | 436.2345 | 326.1 |

**Table S2.** Principal components of the chemical shift tensor ($\delta_{11}$, $\delta_{22}$ and $\delta_{33}$ ppm), isotropic chemical shift ($\delta_{iso}$, ppm), span ($\Omega$, ppm) and skew ($\kappa$).

| | $\delta_{11}$ | $\delta_{22}$ | $\delta_{33}$ | $\delta_{iso}$ | $\Omega$ | $\kappa$ |
|---|---|---|---|---|---|---|
| $PH_3$ | -227.7 | -285.3 | -285.3 | -266.1 | 57.6 | -1.00 |
| POSS-Me terminated | 159.0 | 158.4 | -100.4 | 72.3 | 259.4 | 1.00 |
| POSS-Phosphonate | 65.2 | 21.8 | -196.4 | -36.5 | 261.6 | 0.67 |
| POSS-Phosphonate-silanol | 59.9 | 16.1 | -159.3 | -27.8 | 219.2 | 0.60 |
| POSS-Phosphonate-bis-silanol | 50.9 | 10.0 | -146.2 | -28.4 | 197.0 | 0.59 |
| POSS-Phosphonate-tris-silanol | 55.1 | 7.0 | -134.3 | -24.1 | 189.3 | 0.49 |

**Table S3.** Calculated P-H stretching frequency v(P-H) ($cm^{-1}$) and frequency shift Δv ($cm^{-1}$) generated by the interaction with silanol groups.

| | **v(P-H)** | **Δv** |
|---|---|---|
| POSS-Phosphonate | 2475 | 0 |
| POSS-Phosphonate-silanol | 2498 | +23 |
| POSS-Phosphonate-bis-silanol | 2510 | +35 |
| POSS-Phosphonate-tris-silanol | 2516 | +41 |

**SI 3.** $^{1}$H MAS and $^{13}$C CP-MAS spectra of **POSS-P/SiO$_{2\text{-}(500)}$**

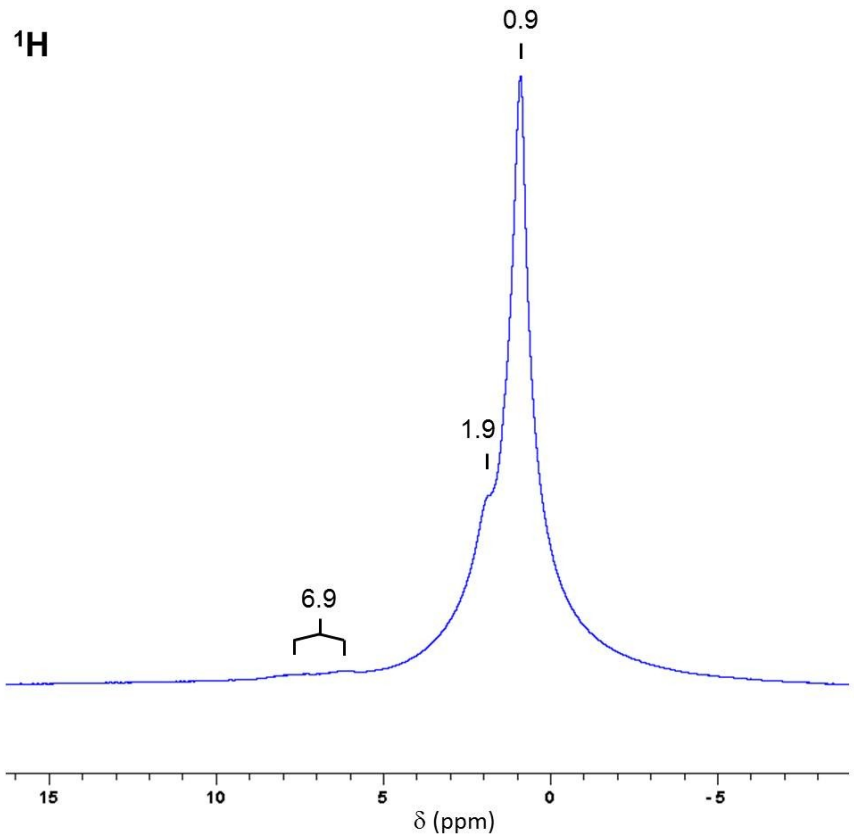


**Figure S3-1.** $^{1}$H MAS solid-state NMR spectrum of **POSS-P/SiO$_{2\text{-}(500)}$** (500 MHz, $\omega_{rot}/2\pi$ = 10 kHz, 8 scans, recycle delay 5 s).

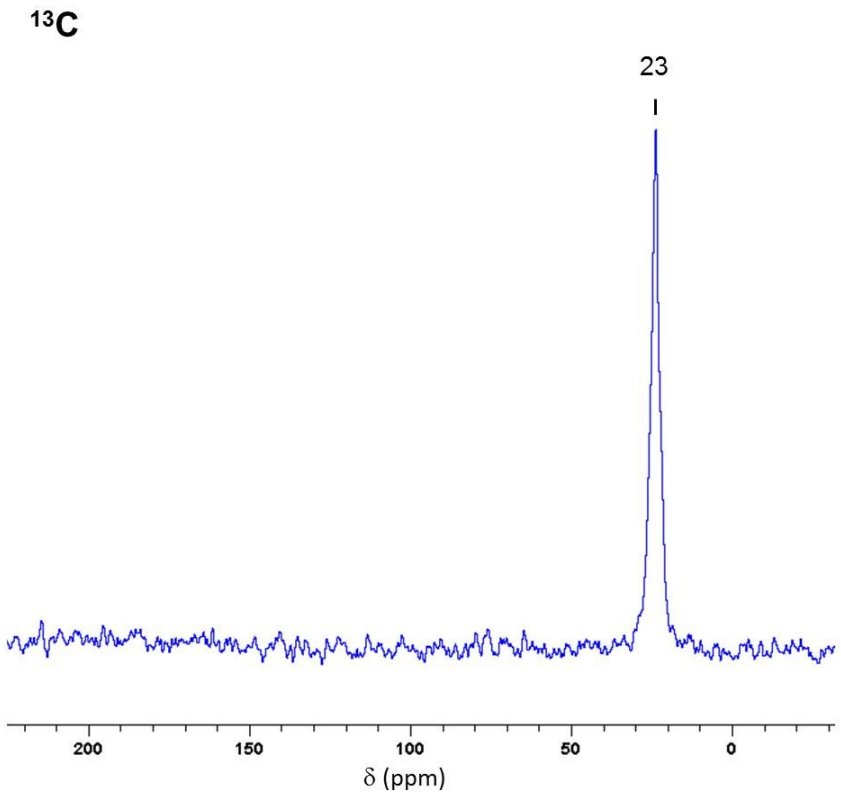


**Figure S3-2.** $^{13}C$ CP-MAS solid-state NMR spectrum of **POSS-P/SiO$_{2-(500)}$** (500 MHz, $\omega_{rot}/2\pi$ = 10 KHz, 4 k scans, recycle delay of 2 s, 2 ms contact time).

**SI 4.** DNP enhanced 2D $^{31}$P magic angle turning (MAT) correlation spectrum of **POSS-P/SiO$_{2\text{-}(700)}$**.

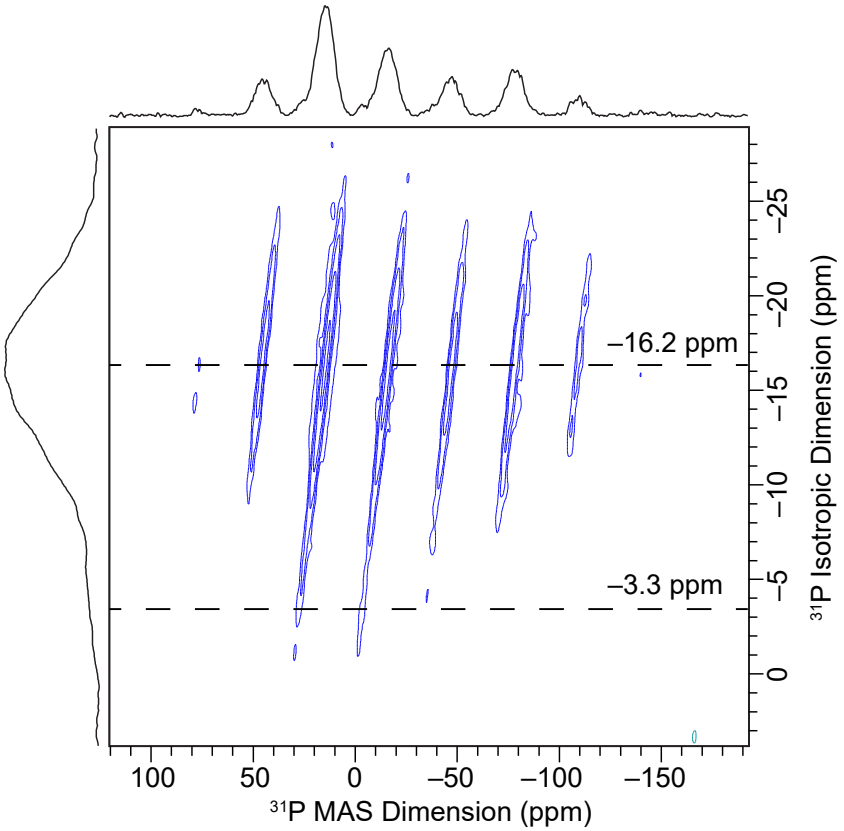


**Figure S4-1.** DNP enhanced 2D $^{31}$P magic angle turning (MAT) isotropic-anisotropic chemical shift correlation spectrum of POSS-P/SiO$_{2\text{-}(700)}$. Slices at isotropic chemical shifts were extracted at –3.3 ppm and –16.2 ppm and are shown in Figure S4-2. The spectrum was acquired with a MAS frequency of 5000 Hz, 14 scans, a 3.0 s polarization delay between scans, 48 $t_1$ increments and a $t_1$ increment of 158.33 ms. The five p pulse MAT sequence of Grant and co-workers was used.[13] Echo-anti-echo acquisition was used to obtain a pure adsorption mode 2D spectrum.

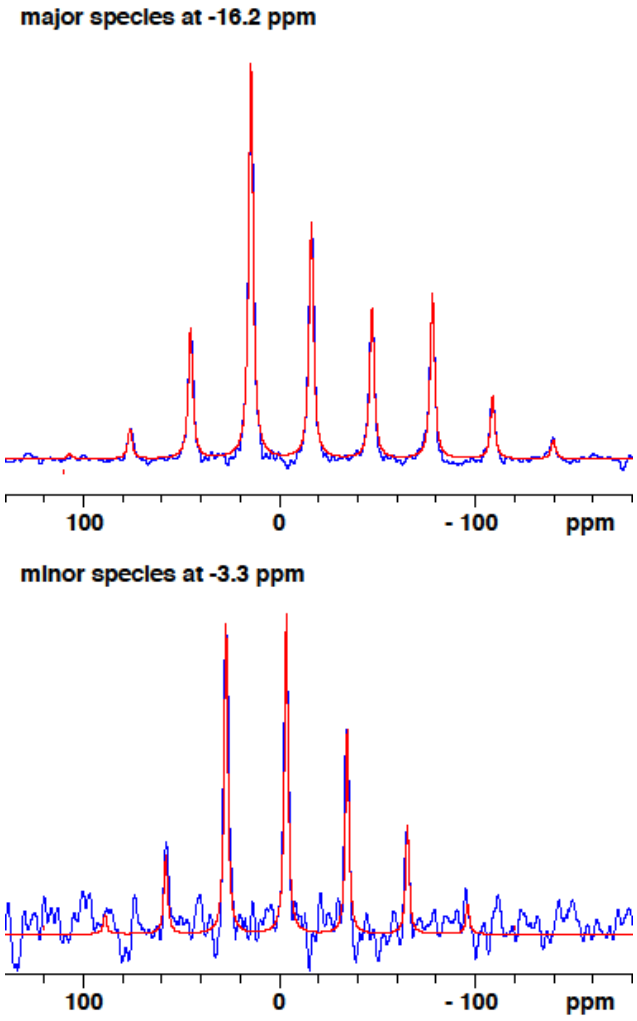


**Figure S4-2.** Slices at isotropic chemical shifts of –3.3 ppm (lower traces) and –16.2 ppm (upper traces) from the 2D $^{31}$P MAT solid-state NMR spectrum (Figure S4-1) and fits of the sideband manifolds (red traces) to obtain the CS tensor parameters (Figure S4-2).

**SI 5.** $^{29}$Si CP-MAS NMR spectra of **POSS-P/SiO$_{2-(500)}$** after grafting and inert or oxidative post-treatment.

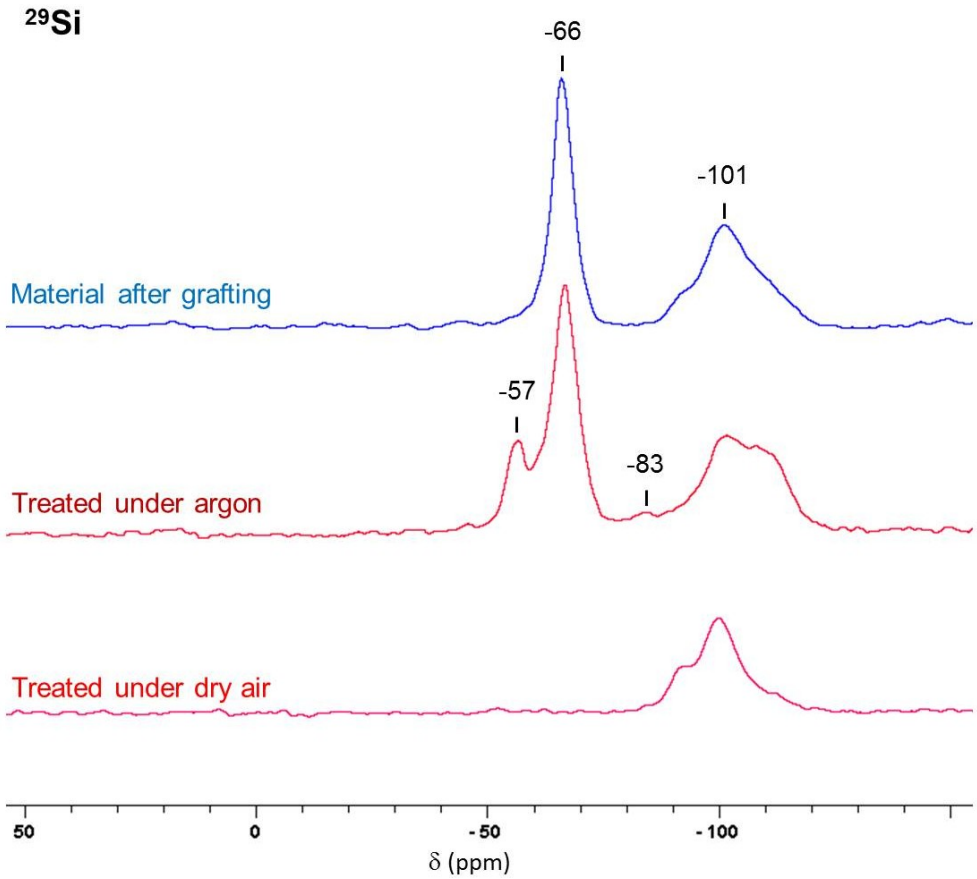


**Figure S5.** $^{29}$Si CP-MAS solid state NMR spectra of **POSS-P/SiO$_{2-(500)}$** after grafting, and treated under argon (inert) or dry air (oxidative atmosphere). 300 MHz, $\omega_{rot}/2\pi$ = 5 KHz, 27 k scans, recycle delay of 2 s, 2 ms contact time.

Spectrum of the sample treated under argon (inert conditions): the peak at -57 ppm ($T_2$-type Si-OH of POSS) shows that the POSS cage is partially opened. The peak of low intensity at -83 ppm reveals the presence of $T_3$-like Si-H of POSS,[14] consistent with the release of small amounts of $C_3/C_4$ alkenes,[15] observed from ~380 °C, and generating Si-H groups (see ν(Si-H) ~ 2250 cm$^{-1}$ on the IR spectrum (main text)).

**SI 6.** DNP enhanced 2D $^{29}$Si-$^{31}$P NMR correlation spectrum of **POSS-P/SiO$_{2\text{-}(700)}$**.

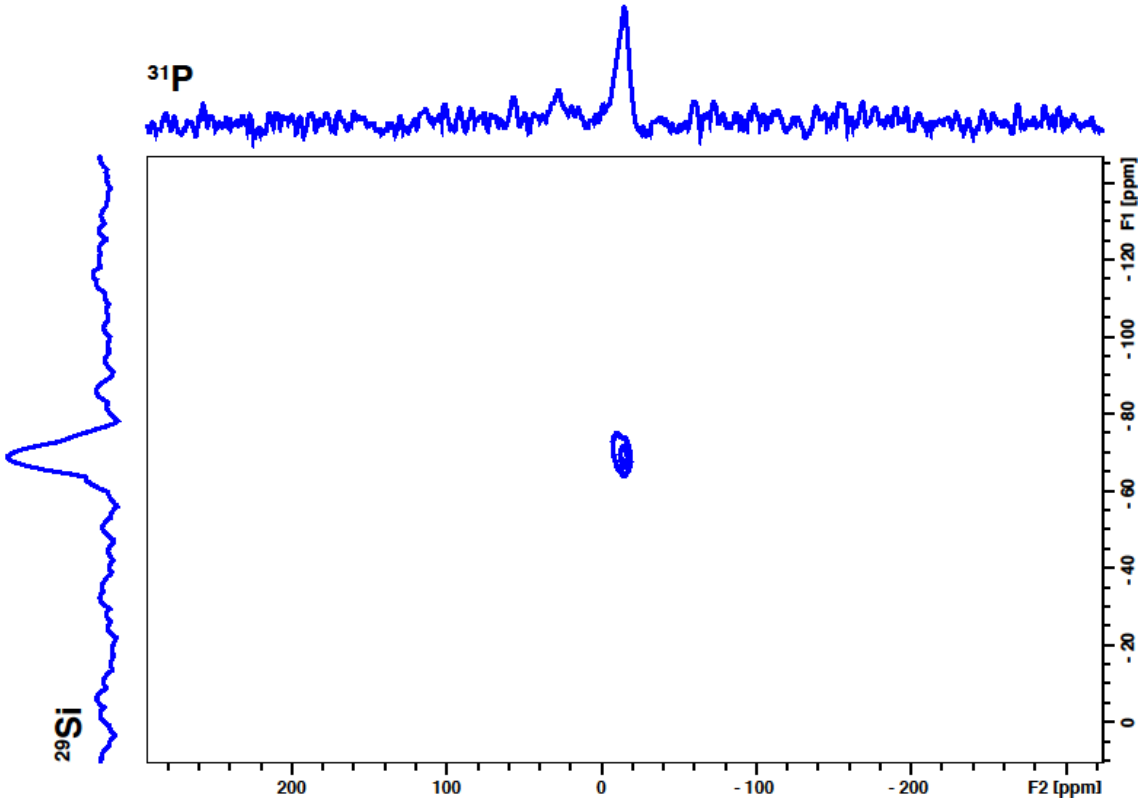


**Figure S6.** DNP enhanced 2D transferred echo double resonance (TEDOR) $^{29}$Si-$^{31}$P correlation spectrum. $^{29}$Si was polarized with a CP step (6 ms contact time), then allowed to evolve for $t_1$. The $^{29}$Si polarization was then transferred to $^{31}$P for detection with REDOR recoupling. 80 total rotor cycles of recoupling (6.4 ms) was used for $^{29}$Si-$^{31}$P coherence transfer. The States-TPPI procedure was employed to obtain phase sensitive detection. The spectrum was acquired with a MAS frequency of 12500 Hz, 24 scans per $t_1$ increment, a rotor synchronized 80.0 μs $t_1$ increment and 24 total $t_1$ increments.

**SI 7.** Stability of surface species upon inert or oxidative thermal treatment, and followed by *in-situ* IR coupled with GC/MS.

**Details:** FT-IR spectra recorded in DRIFT mode were obtained on a Nicolet 6700 FT-IR spectrometer. The samples were loaded into a custom DRIFT cell equipped with ZnSe windows under inert atmosphere (glovebox). Typically, 4 spectra per minute were acquired, with 64 scans (4 $cm^{-1}$ resolution). POSS-P/$SiO_2$ (typically 20 mg) was decomposed under a flux (10 ml/min) of dry gas (air or $N_2$), with a heating rate of 3°C.$min^{-1}$, from ~20°C to 500°C, and maintained at 500°C for 2h before being cooled to the starting temperature. Gases, released during thermal treatment, were collected and analyzed by GC/MS for identification.

**Decomposition under inert atmosphere ($N_2$):**

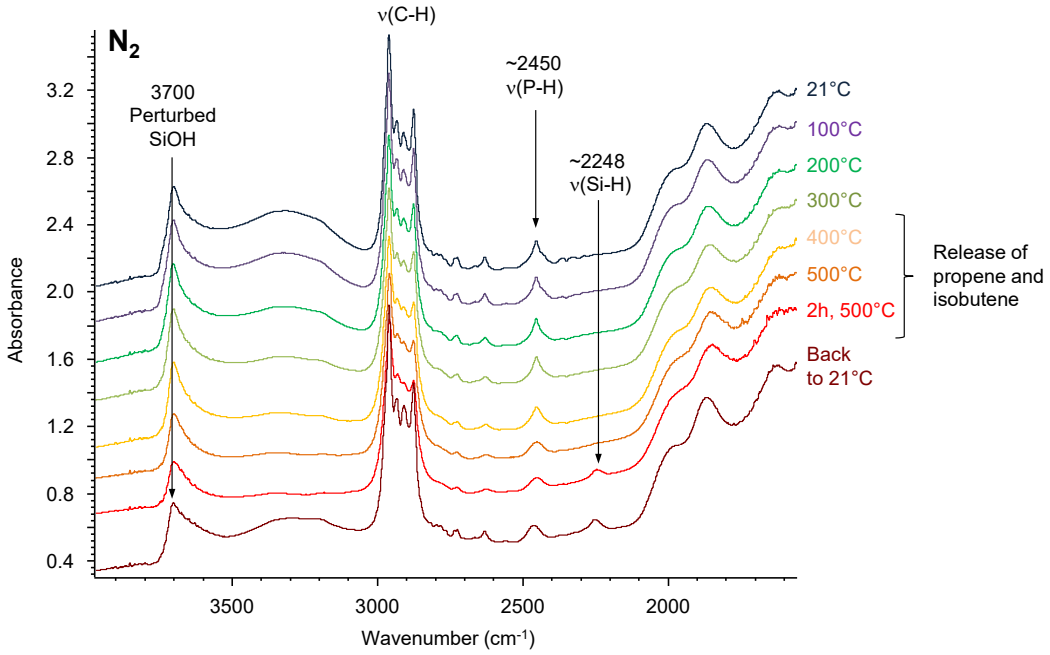


**Figure S7-1.** IR (DRIFT) spectra of POSS-P/$SiO_2$ decomposed under dry and $O_2$-free $N_2$, between 21°C and 500°C.

**Decomposition under oxidative atmosphere (air):**

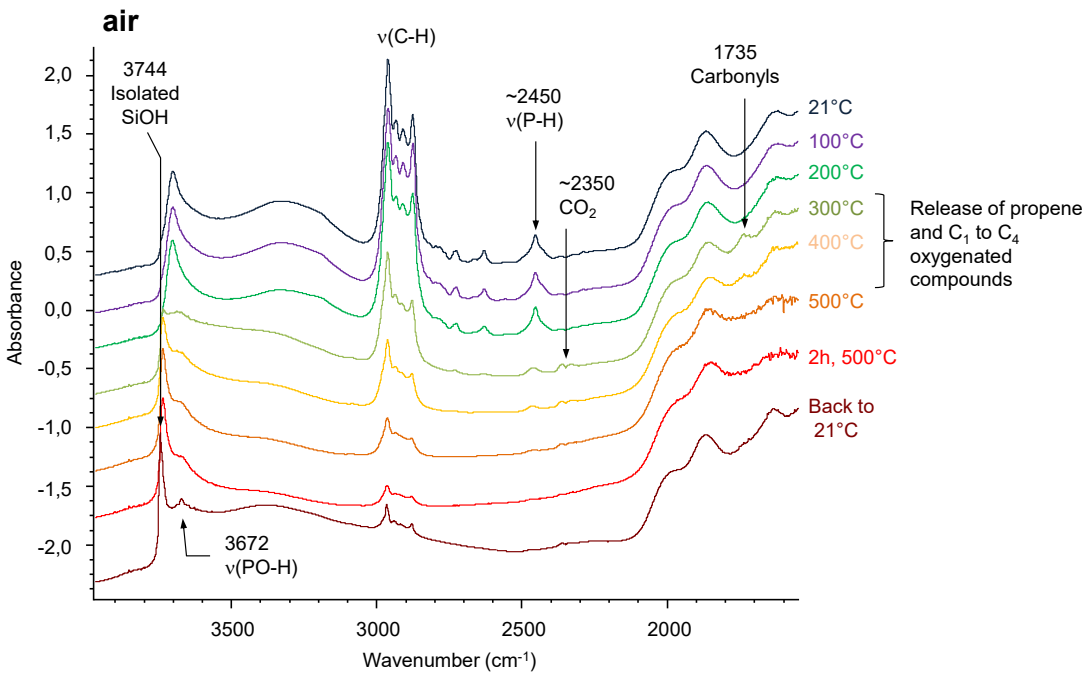


**Figure S7-2**. IR (DRIFT) spectra of POSS-P/$SiO_2$ decomposed under dry air, between 21°C and 500°C.

**SI 8.** $^{31}P\{^{1}H\}$ pulse-acquire MAS spectra of **POSS-P/SiO$_{2-(500)}$** after grafting and inert or oxidative post-treatment.

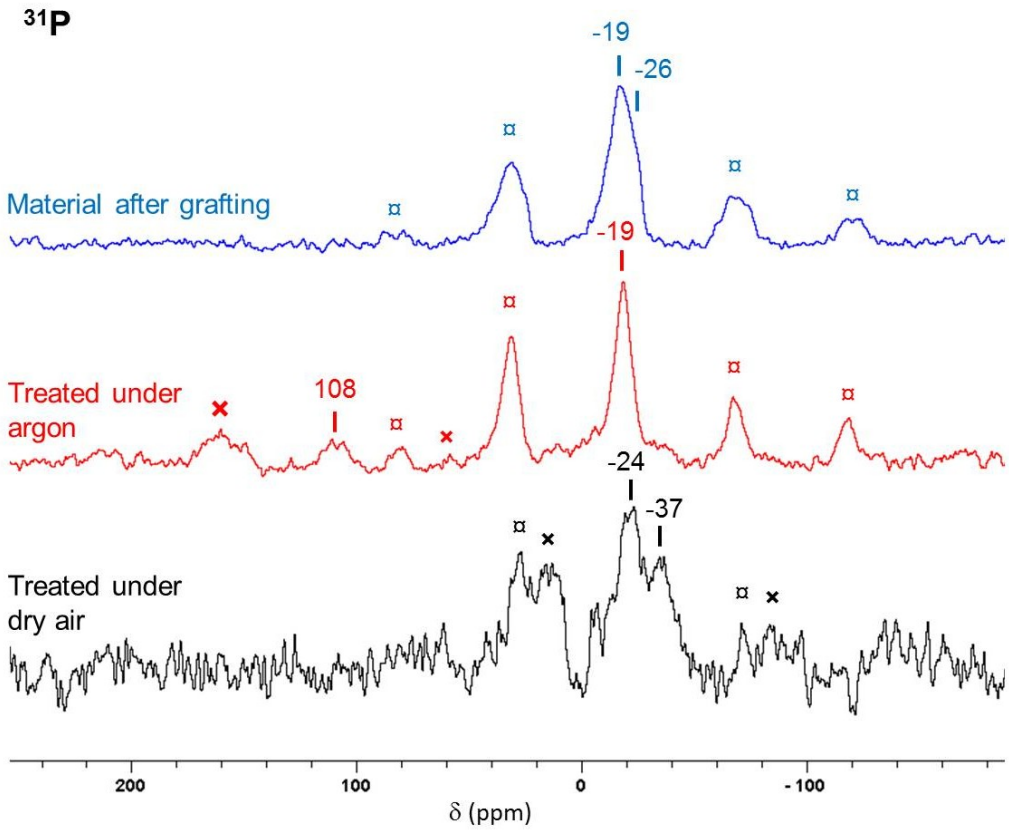


**Figure S8.** $^{31}P$ pulse-acquire, $^{1}H$ decoupled MAS solid state NMR spectra of **POSS-P/SiO$_{2-(500)}$** after grafting, and treated under argon (inert) or dry air (oxidative atmosphere). 500 MHz, $\omega_{rot}/2\pi$ = 10 KHz, from 1 k to 3 k scans, recycle delay 40 s, except for the sample treated under dry air (100 s). ¤ and × denote spinning side bands.

**SI 9.** Secondary ion mass spectrometry (SIMS) depth profiles of carbon in silicon

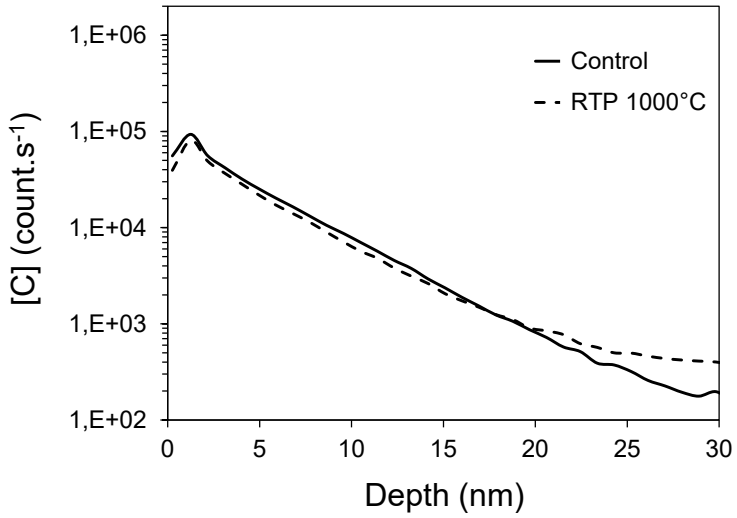


**Figure S9.** Secondary ion mass spectrometry (SIMS) depth profile of carbon from P-grafted wafers and a reference (control) non-doped wafer annealed in the same conditions (spike 1s, 1000°C, 1.5 nm $SiO_2$).

The tail observed on both depth profiles of carbon in silicon (control and sample) is an artifact coming from the use of a $Cs^+$ ion beam for sputtering.

## **SI 10.** References


(1) Rosay, M.; Tometich, L.; Pawsey, S.; Bader, R.; Schauwecker, R.; Blank, M.; Borchard, P. M.; Cauffman, S. R.; Felch, K. L.; Weber, R. T.; Temkin, R. J.; Griffin, R. G.; Maas, W. E. Solid-State Dynamic Nuclear Polarization at 263 GHz: Spectrometer Design and Experimental Results. *Phys. Chem. Chem. Phys.* **2010**, *12* (22), 5850–5860.

(2) Fung, B. M.; Khitrin, A. K.; Ermolaev, K. An Improved Broadband Decoupling Sequence for Liquid Crystals and Solids. *J. Magn. Reson.* **2000**, *142* (1), 97–101.

(3) Agarwala, A.; Subramani, T.; Goldbourt, A.; Danovich, D.; Yerushalmi, R. Facile Monolayer Formation on SiO2 Surfaces via Organoboron Functionalities. *Angew. Chem. Int. Ed.* **2013**, *52* (29), 7415–7418.

(4) Yerushalmi, R.; Ho, J. C.; Fan, Z.; Javey, A. Phosphine Oxide Monolayers on SiO2 Surfaces. *Angew Chem Int Ed* **2008**, *47*, 4440–4442.

(5) Longo, R. C.; Cho, K.; Schmidt, W. G.; Chabal, Y. J.; Thissen, P. Monolayer Doping via Phosphonic Acid Grafting on Silicon: Microscopic Insight from Infrared Spectroscopy and Density Functional Theory Calculations. *Adv. Funct. Mater.* **2013**, *23* (27), 3471–3477.

(6) Schulmeyer, T.; Paniagua, S. A.; Veneman, P. A.; Jones, S. C.; Hotchkiss, P. J.; Mudalige, A.; Pemberton, J. E.; Marder, S. R.; Armstrong, N. R. Modification of BaTiO3 Thin Films: Adjustment of the Effective Surface Work Function. *J. Mater. Chem.* **2007**, *17* (43), 4563–4570.

(7) M. J. Frisch, G. W. Trucks, H. B. Schlegel, G. E. Scuseria, M. A. Robb, J. R. Cheeseman, G. Scalmani, V. Barone, B. Mennucci, G. A. Petersson, H. Nakatsuji, M. Caricato, X. Li, H. P. Hratchian, A. F. Izmaylov, J. Bloino, G. Zheng, J. L. Sonnenberg, M. Hada, M. Ehara, K. Toyota, R. Fukuda, J. Hasegawa, M. Ishida, T. Nakajima, Y. Honda, O. Kitao, H. Nakai, T. Vreven, J. A. Montgomery, Jr., J. E. Peralta, F. Ogliaro, M. Bearpark, J. J. Heyd, E. Brothers, K. N. Kudin, V. N. Staroverov, T. Keith, R. Kobayashi, J. Normand, K. Raghavachari, A. Rendell, J. C. Burant, S. S. Iyengar, J. Tomasi, M. Cossi, N. Rega, J. M. Millam, M. Klene, J. E. Knox, J. B. Cross, V. Bakken, C. Adamo, J. Jaramillo, R. Gomperts, R. E. Stratmann, O. Yazyev, A. J. Austin, R.

Cammi, C. Pomelli, J. W. Ochterski, R. L. Martin, K. Morokuma, V. G. Zakrzewski, G. A. Voth, P. Salvador, J. J. Dannenberg, S. Dapprich, A. D. Daniels, O. Farkas, J. B. Foresman, J. V. Ortiz, J. Cioslowski, and D. J. Fox, Gaussian, Inc., Wallingford CT, 2010. Gaussian 09, Revision C.01.

(8) W. Kutzelnigg, U. Fleischer, M. Schindler. *The IGLO-Method: Ab Initio Calculation and Interpretation of NMR Chemical Shifts and Magnetic Susceptibilities*, Springer-Verlag.; Heidelberg, 1990; Vol. 23.

(9) B. Maryasin; H. Zipse. Theoretical Studies of 31P NMR Spectral Properties of Phosphanes and Related Compounds in Solution. *Phys Chem Chem Phys* **2011**, *13*, 5150–5158.

(10) C. van Wüllen. A Comparison of Density Functional Methods for the Calculation of Phosphorus-31 NMR Chemical Shifts. *Phys Chem Chem Phys* **2000**, *2*, 2137–2144.

(11) Herzfeld, J.; Berger, A. E. Sideband Intensities in NMR Spectra of Samples Spinning at the Magic Angle. *J. Chem. Phys.* **1980**, *73* (12), 6021–6030.

(12) http://cccbdb.nist.gov/vibscale2.asp?method=8&basis=1.

(13) Hu, J. Z.; Alderman, D. W.; Ye, C. H.; Pugmire, R. J.; Grant, D. M. An Isotropic Chemical Shift-Chemical Shift Anisotropy Magic-Angle Slow-Spinning 2D NMR Experiment. *J. Magn. Reson. A* **1993**, *105* (1), 82–87.

(14) Zhang, D.; Liu, Y.; Shi, Y.; Huang, G. Effect of Polyhedral Oligomeric Silsesquioxane (POSS) on Crystallization Behaviors of POSS/polydimethylsiloxane Rubber Nanocomposites. *RSC Adv* **2014**, *4* (12), 6275–6283.

(15) Fina, A.; Tabuani, D.; Carniato, F.; Frache, A.; Boccaleri, E.; Camino, G. Polyhedral Oligomeric Silsesquioxanes (POSS) Thermal Degradation. *Thermochim. Acta* **2006**, *440* (1), 36–42.